ISSN: 2634 - 8853

Journal of Engineering and Applied Sciences Technology

SCIENTIFIC Research and Community

Editorial Article

Open Access

# Systematic Study about the Elemental Interference in Phosphotungstate Structure in Ormosil Films

**Orlando Elguera Ysnaga**

Institute of Chemistry of Sao Carlos, University of Sao Paulo (IQSC-USP), Sao Carlos-SP, Brazil

## ABSTRACT

XRF measurements in ormosil, performed at laboratory equipment, showed us the self-absorption effect of the Tungsten fluorescence by Phosphorous in the phosphotungstates. However, in the extent that increase the Zn concentration in ormosil, the Phosphorous absorption effect decreases gradually. EDXRF measurements of ormosil films containing phosphotungstates ($[PW_{12}O_{40}]^{-3}$) showed that there is an inverse correlation between the concentrations of Phosphorous and Tungsten, or that the concentration of Phosphorous was overestimated and the concentration of Tungsten has been underestimated. In order to explain this phenomenon, they were performed studies of mixed solutions of phosphates and tungstates, Studies done with molybdates solutions showed the same trend than tungstates ones, analogously. Thus, we concluded that the structure of polyoxometalates (phosphotungstates and phosphomolybdates), containing Phosphorous as central atom, has influence on XRF analysis because the results obtained in tungstates and molybdates solutions. In the extent that the Phosphorous atoms are closer to Tungsten and/or Molybdenum ones, the probability of interaction between them will enhance. Thus, the interference of Phosphorous in X-ray Fluorescence of Tungsten and/or Molybdenum will be increase, thereby simulating the existing proximity of these elements in the molecules of the phosphotungstates and phosphomolybdates. Self-absorption/interference studies of Tungsten X-ray Fluorescence by the others constituents in the ormosil films led us to approach the XRF quantification not only from the atomic perspective, but also to supplement with the molecular approach. We proposed an interference model that takes into account the self-absorption of the Tungsten fluorescence by Phosphorous, the cage-shaped molecular structure (Keggin) of the polyanions and their distribution in the structure of ormosil. Considering that the Tungsten and Phosphorous main emission lines do not overlapping by EDXRF, were performed measures by WDXRF finding the superposition of Tungsten W-$L_{G4}$ and Phosphorous P-Kα lines, but that is not enough to justify our experimental observations. Therefore, we regarded an additional explanation, the X-ray Resonant Raman Scattering produced by the $O^{2-}$ anions network in phosphotungstates, followed of the Phosphorous absorption of the inelastic scattered photons for the $O^{2-}$ anions. Thus, the interference does not occur primarily by direct self-absorption, but by a combination of inelastic scattering process followed by absorption. The increase in X-ray fluorescence of Phosphorous in phosphotungstates could be due to various phenomenon such as Secondary Fluorescence, X-ray Resonant Raman Scattering and by the contribution of radiative satellites Auger lines. XANES and EXAFS measurements given evidence of intermolecular and intramolecular interaction between Zinc and Tungsten species.

***Corresponding author**

Orlando Elguera Ysnaga, Institute of Chemistry of Sao Carlos, University of Sao Paulo (IQSC-USP), Sao Carlos-SP, Brazil.

**Received:** March 08, 2025; **Accepted:** March 11, 2025; **Published:** March 21, 2025

**Keywords:** XRF-Phosphorous Interference, XANES-EXAFS, XRRS, Auger Effect, Secondary-XRF

## Introduction

Ormosil (Organic Modified Silicates) are hybrid materials whose contain as inorganic part a matrix host composed by 3-D silicates bearing silanol and siloxane bonds (-Si-OH- and-Si-O-Si respectively), as well as -Si-C- bonds and organic functionalities (X groups, for example amino, nitrile, alkyl and aryl groups). The chemical nature of the organic groups has a strong impact on the physical and chemical properties of these class II hybrid materials. The ormosil, we are studying, are composed of silicates organically modified with amino, nitrile, diol and ether functionalities, containing phosphotungstic acid ($H_3PW_{12}O_{40}.XH_2O$, also namely PWA) doped with Titania ($TiO_2$) nanoparticles or Zinc ions ($Zn^{2+}$). Therefore, the elements occurring in these materials are C, H, O, P, Zn, Ti and W. These materials are photoactive, presenting enhanced behavior in their photochromic and photo-catalytic properties as function of the dopant concentration [1,2]. The ormosil are prepared by Sol-Gel process. In Sol-Gel process chemistry, the particles may growth without becoming crystalline and, even in cases where they are crystalline, line-broadening and disordered regions near the surfaces of the very small crystals may greatly complicate detailed structural characterization by conventional X-ray crystallography. In such circumstances, XAFS (XANES and EXAFS) measurements of ormosil (hybrid materials) must help us to enlighten a few questions on XRF suppression of Tungsten and enhancement of Phosphorous, as well as allow understanding the Zn and Ti environmental coordination [3]. XAFS is one of the most powerful tools we have for mapping local structure, especially for non-crystalline materials such the ormosil. X-ray Absorption Fine Structure (EXAFS) analyses could be very valuable in order to characterize the local environment of ormosil during processing. In previous photochromic studies, we have been able to observe remarkable enhancement of the photochromic properties of ormosil films doped with Zinc cations. Nevertheless, no clear explanation

for such enhancement were provided by P and Si MAS-NMR, FTIR (MIR and NIR), Raman spectroscopy and XRD. The deeper understanding of the mechanism involved in such enhancement process require the determination of the local structure of the W and Zn elements, therefore the combined EXAFS and XANES spectra can shadow light in this process. Moreover, XRF spectra of the ormosil samples display unusual interference of Si, Ti and Zn on the W emission. No direct absorption process of the photon emitted by the W cations in the matrix is expected, thus inelastic scattering of the W emitted photons and further absorption of the slowed down photon arise as a possibility. Such hypothesis would be only valid, if in the neighborhood of the W cations we could have Si, Zn or Ti species. Therefore, EXAFS should be a technique of choice in order to achieve this goal.

**Previous Characterization of Ormosil Films by other Techniques**

Photochromism measurements of the ormosil films using electronic optical spectroscopy showed up 350% of increase in the photochromic response to UV irradiation due to Zn presence. FTIR and Raman measurements with and without Ti and Zn allow the characterization of the organic functionalities and the phosphotungstate oxo-cluster, as well as P and C P MAS-NMR measurements. Interpenetrating network polymer formation was confirmed by C P MAS-NMR analysis. Small shifts in the infrared peaks corresponding to W-O-W, present in the phosphotungstate, suggests an ion-pair formation between the protonated TiO2 surface and the phosphotungstate ions, however no shift was observed in the $Zn^{2+}$ doped ormosil. TEM images have shown that there are $Zn^{2+}$ and $TiO_2$ nano-domains in ormosil. WAXS measurements displayed a non-crystalline diffractogram with a few broad diffraction peaks overlapped to amorphous halo, which were assigned to the undergoing lamellae formation and/or oligo-silicate cage formation. SAXS measurements indicate the presence of Titania particles; nevertheless, none ZnO was observed for the Zn2+ doped ormosil. For these reasons, we need to perform XAFS measurements that will complement the information about the spatial distribution of the elements Ti and Zn obtained by TEM as also explain the absorption effect (Si, P, W) that happens in XRF measurements.

The X-ray spectrum depends on the kind of elementary process occurring in the active atom and on the surrounding atoms [4]. The process resulting in X-ray emission can be studied by measuring the wavelength dependence of the intensity and in turn the intensity dependence with the kinetic energy of the exciting electrons [4]. X-ray emission spectrum is based on the Bohr's model. However, this model cannot explain all the several structures found in emission spectra, as in the case of X-ray non-diagram lines or satellites, X-ray emission bands and vibrational structures, generated by the production of inner or outer vacancies in molecules.

According to Liebhafsky: "*In modern theories of the solid state, the outer electrons are regarded as belonging to the entire solid, occupying bands of electronic states characteristic of the entire solid*" [5]. In the model of Bands, the orbitals in the solid (called Bloch functions also) are created from the linear combination of atomic orbitals. Thus, the energy of these orbitals in the crystal is function of the energy of the correspondent atomic orbitals used in the linear combination. Therefore, any electronic transition involving these bands has its energy dependent, not only of the chemical composition, but also of the symmetry of the compound formed, similar to the case of molecular orbitals in the molecules [6]. The dependence of the intensity and energy in an X-ray emission or absorption spectrum, with the molecular and/or crystalline structure, in which the motion of valence electrons is perturbed by the surrounding (because of orbital dimensions and interatomic distances) is justified to the extent that the Bloch's orbitals exhibit a different symmetry than atomic orbitals. Thus, this difference in symmetry results in different electronic transitions moments, similar to what occurs with the absorption and emission molecular spectra in the region corresponding to UV-vis [7].

According to Meisel et al: "*The X-ray absorption spectrum reflects the wavelength-dependence intensity reduction produced by inelastic interaction of X-ray photons" as also that "this spectrum displays prominent absorption edges, with accompanying manifolds of fine-structure features*". The elementary process of absorption depends upon the probability that an atom captures an X-ray photon incident upon it; being that this probability governs the value of the mass absorption coefficient. This probability is function of the number and kind of atoms that the photon encounters in its path.

**X-Ray Satellites**

There are several different possibilities for the origin of the X-ray satellites. Between the possibilities are satellites from multiplet splitting (lines emitted from atoms with unfilled d or f subshells), and satellites from multiplet cross-transitions (weaker maxima near the main emission bands in molecules and solids).

**Objective**

- Develop an explorative study of the interference of the Phosphorous on the Tungsten fluorescence in phosphotungstates contained in ormosil films.
- Determine by EXAFS measurements the chemical environment of Zn, Ti and W in ormosil, by means of the knowledge of the bond lengths between (W–Zn), (W–P), and (W-Si) in function to Zn concentration as also to determine the coordination number of Tungsten in order to enable us to know if there is an intra-atomic or interatomic interaction between the Zn and W.
- Determine by XANES measurements the electronic state of chemical element Tungsten (W) in ormosil.

**Theory**

The X-ray emission spectra consist of intense diagram lines, satellites or weak lines, and emission bands [4]. The satellites are caused by simultaneous electronic transitions from normally unoccupied outer orbitals to inner vacancies in multiply ionized atoms, from many-electron processes, by multiplet splitting of X-ray terms (lines emitted from atoms with unfilled d or f sub-shells) and by the modifications of the atomic energy levels due to the chemical bonding. The X-ray emission bands from an element in molecules and solids, originate from mixing valence orbitals of the emitting atom with orbitals from the surrounding atoms, in contrast to isolated atoms, show totally different (in shape) intensity distributions.

**Non-Diagram Lines**

Non-diagram lines are called to those weak lines observed in X-ray spectra whose frequencies cannot be expressed as difference of spectroscopic terms. Siegbahn and Stenström first established the presence of such lines in the K spectra of the elements Cr to Ge in 1916. These lines are often close to strong diagram lines and hence are frequently referred as satellites. In the K series (Kα and Kβ groups), defined satellites have been found in elements from Na to Ge. In the L series ($L_{\alpha 1}$, $L_{\beta 1}$ and $L_{\beta 2}$), the stronger lines have satellites for the elements with Z< 50. In the M series ($M_{\alpha 1}$,

Mβ and Mγ), non-diagram lines were first reported by Hjalmar in 1923. The chemical environment of the emitting atom, as its chemical bonding influence the relative intensities and energies of X-ray satellites lines.

Due to that the lifetime of an X-ray state (on the order of magnitude of $10^{-18}$ seconds) is smaller than the relaxation time for electrons in outer shells for atoms of higher atomic number, so that excited states occur with energies higher than those normal X-ray states. The first theoretical attempt to explain the presence of these non-diagram lines was made by Wentzel in 1921. He assumed that these lines were result of single electron jumps in atoms having two or more inner electrons removed. Druyvenstein in 1927 modified the Wentzel's theory in such a manner that is not necessary suppose the loss of two electrons from an n, l, shell. F.K Ritchmeyer in 1929 suggested another explanation of the satellites, based on the idea of double electron jumps. According to his theory, valid mainly for the K satellites: "*the satellite line is due to the simultaneous transition of an inner and an outer electron, from a higher to a lower energy level, so that the energy of the emitted quantum is the sum of both energy differences". For the "parent" line, only the transition of the inner electron should be responsible*" [8]. Coster and Kronig in 1935 have succeeded in giving a satisfactory explanation of the L satellites (and its dependence on Z), due to the Auger emission of an M electron and the simultaneous non-radiative transition of an L electron from (2p) to (2s) level. BLocH has discussed the simultaneous emission of a light quantum and an outer electron (radiative Auger effect), given as example the occurrence of the Cu Kα3 satellite, developing a formula for the probability of double transitions by dipole radiation. Lower-energy lines, such as the observed by Das Gupta' and Suzuki et al., have been attributed to a Compton-Raman type of scatter, in which a bound electron recoils with just enough energy to be ejected, leaving the photon reduced in energy by the binding energy of this ejected K electron [9].

**Radiative Auger Effect**

According to Liebhafsky: "*Inasmuch as the Auger effect can occur in any atom having a single appropriate electron hole, also are produced satellites lines by electron excitation*". An X-ray inner-hole state decays through a radiative (Fluorescence), a nonradiative (Auger) transitions and other modes. Bloch suggested in 1935 that an atom might be able to emit an X-ray photon and a valence-shell electron simultaneously, instead of undergoes a "forbidden" quadrupole transition; as also gave a rough estimate of the probability of the radiative Auger effect, where these transitions replace the dipole forbidden X-ray transitions [10,11]. Åberg et al in 1969 reported the observation of another possible decay mode, called "radiative Auger effect" or "atomic internal Compton effect", to one in which a photon and an inner L-shell electron are emitted simultaneously instead of the dipole allowed (Kα line) in Mg, Al, Si, and S. The electron may also be excited into a bound state during the X-ray emission process.

**X-Ray Resonant Raman Scattering (XRRS)**

The spectrum of scattered radiation, produced by monochromatic X-rays, consists of the Rayleigh line, Compton band and Raman lines. These latter reflect the different photon energies produced by inelastic scattering from bound electrons of the scattering material. The X-ray Raman scattering is a second order process of the photon–atom interaction, in which a core-electron is excited into an unoccupied state, above the Fermi level, by the absorption of a photon [12]. This intermediate "virtual" state of the neutral atom decays via radiative mechanism, the initial core hole being filled by another inner-shell electron. The cross section for Raman scattering is generally extremely small compared to the elastic (Rayleigh) scattering. Sparks and Eisenberger et al. performed pioneering works on the X-Ray Resonant Raman Scattering (XRRS), using X-ray tubes and synchrotron radiation respectively, in the 1970s. Due to its resonant character, the XRRS is a powerful method in order to study the electronic structure of solids, being complementary to the X-ray absorption techniques based on the first-order process.

The X-Ray Resonant Raman Scattering occurs when the incident radiation has an energy value close to the corresponding X-ray absorption edge of the element that we wish to determine [9,13]. Under these conditions, the cross-section of that scattering increases significantly, being able to be of the same magnitude of the cross section for elastic (Rayleigh) scattering.

According to Schülke (2007) the X-Ray Resonant Raman Scattering depends on the electronic structure of the material [14]. Bergmann et al. (2002) showed the application of this spectroscopy, in order to complement the information provided by XANES spectra for light elements (Z <10) [15].

In 2012, Sánchez et al reported, through of theoretical calculations, the influence of the X-Ray Resonant Raman Scattering contributions to the background of X-ray fluorescence spectra, therefore in XRF analysis, including enhancement processes [16]. This influence is important, using monochromatic incident radiation, for light elements in low and trace concentration levels, and if these are closer in Atomic Number.

**Chemical Influences in X-Ray Absorption and Emission**

According to Liebhafsky: "*In most of cases the X-ray spectra are in a first approximation independent of the chemical combination (chemical influences) of the emitting of absorbing atom, because these processes involve energy levels close to the nucleus*". However, slight changes (*chemical influences*) in the emission and absorption spectrum have been found *at very high resolution* and attributed to chemical effects [5,7,17]. Bergengren was the first who demonstrate an effect of chemical combination of Phosphorous, in various allotropic modifications, found slight variations in the wavelength of the absorption edge spectrum. Lindh and Lundquist were the first in to discover an effect of chemical combination in X-ray spectra at the Kβ1 line of P, S and Cl in various compounds. For Chlorine, Lindh found that there are characteristic emission lines patterns for all the chlorides ($Cl^-$), chlorates ($ClO_3^-$), and perchlorates ($ClO_4^-$). Wetterblad investigated the Kβ group of Na, Mg, Al, and of their correspondent oxides, found differences. According to Liebhafsky: "*The chemical influences are more pronounced in the region of low atomic numbers, in which the valence shells are nearer to the nucleus", as also that "Chemical influences affect the fine structure, causing shifts in wavelength, and thus, changes in the intensity-wavelength distribution*".

The influence of chemical binding, oxidation state, electronegativity of the surrounding atoms and the coordination number on the wavelengths and shape of the Kα1,2 doublet of the elements of the third period is evident from the shifts of lines towards shorter wavelengths, arising when the positive charge of the atom under study increases.

**Experimental Section**

**Instrumental Section**

Energy Dispersive X-Ray Fluorescence Spectrometry (EDXRF)

The ormosil samples were analyzed by the following Energy Dispersive X-Ray Fluorescence (EDXRF) spectrometers:

- Minipal-4 Model PW4025 Panalytical benchtop EDXRF spectrometer, equipped with one 9W Rh X-ray tube and SDD detector (resolution~145eV) at Analytical Center of the Instituto de Química de São Carlos from the Universidade de São Paulo (IQSC-USP). The experiments were done under Helium and air atmosphere; the acquisition time per sample was 450 seg. It was used the Omnian software, in order to perform semi-quantitative determination. The XRF lines of Silicon (Si), Phosphorous (P), Titanium (Ti), Zinc (Zn) and Tungsten (W) chosen were: Si-Kα (1.740 keV), P-Kα (2.010 keV), Ti-Kα (4.510keV), Zn-Kα (8.637keV), and W-Lα (8.396keV) respectively. They were performed three measurements per sample.

- Cartesian Geometry Model NEX CG Rigaku benchtop EDXRF spectrometer- equipped with one 50W Pd X-ray tube and high performance SDD detector at Laboratory of X-ray Diffraction and X-ray Fluorescence of the Rigaku-São Paulo-Brazil. The experiments were done under Helium atmosphere; the acquisition time per sample was 1200 seg, and the concentrations obtained by the use of Fundamental Parameter (FP) method using the RPF-SQX software, that features the Rigaku Profile Fitting (RPF) technology (Moriyama et. al 2011).

**Wave Dispersive X-Ray Fluorescence Spectrometry (WDXRF)**
The WDXRF measurements for Zinc and Tungsten contained in the ormosil samples were performed at the WDXRF Rigaku Model RIX-3000 spectrometer- equipped with one 3kW Rh X-ray tube, LiF 200 crystal analyzer and scintillation counter detector (SC) at Laboratory of X-ray Fluorescence of the Centro de Química e Meio Ambiente (CQMA) from Instituto de Pesquisas Energéticas e Nucleares (IPEN/CNEN-SP). The experiments were done under Helium atmosphere; the acquisition time per sample was 2700 seg. The XRF lines of Zinc (Zn) and Tungsten (W) chosen were (in 2θ angle units): Zn-Kα (41.75°) and W-Lα (43.00°) respectively. They were performed three measurements per sample.

**X-Ray Absorption Near Edge Structure (XANES)**
XANES spectra at the W LIII edge (10.199 eV), Zn K-edge (9.659 eV) and Ca K-edge (4.034 eV) were collected in transmission mode for the reference compounds (dissolved in Boron Nitride pellets) and in fluorescence mode for the samples (ormosil films deposited on Si [111] wafers). The spectra of W LIII-edge were recorded between 10120-10268 eV with energy steps of 2.0 eV (10120-10200 eV) and 0.3 eV (10200-10268 eV). The spectra of Zn K-edge were recorded between 9.590-9.800 eV, with energy step of 0.5 eV; and the spectra of Ca K-edge were recorded between 3900-4098 eV, with energy steps of 2.0 eV (3900-4028 eV) and 0.5 eV (4028-4098 eV). For these measurements were used a Si (111) double-crystal monochromator and a Ge-15 SSD detector (with resolution (ΔE/E): 1.71 x 10-4 at 7 keV) at the D08BXAFS2 beamline of the LNLS (National Synchrotron Light Laboratory) facility, Campinas-Brazil. The beam size (HxV) was 450 x 250 $\mu m^2$ with energy range: 4-17 keV.

**Extended X-Ray Absorption Fine Structure (EXAFS)**
EXAFS spectra were collected in transmission (for reference compounds) and fluorescence (for samples) modes, using a Si (111) double-crystal monochromator at the D08BXAFS2 beamline of the LNLS (National Synchrotron Light Laboratory) facility, Campinas-Brazil. EXAFS spectra at the W LIII-edge were recorded between 10100 and 11000 eV using an energy step of 2 eV. The extraction and analysis of EXAFS spectra were performed using the CHEROKEE software 2.5 version and for the corresponding simulating the Roundmidnight package (Roundmidnightfit 2.0 version and RoundmidnightRev 3.1 version software).

**Samples and Certified Reference Materials**
**Samples:** the samples analyzed were:
- Ormosil films containing phosphotungstates doped with TiO2. Sample's Code: SNP, A2, A6, A7, A8.
- Ormosil films containing phosphotungstates doped with ZnO. Sample's Code: Z1.0, Z0.5, Z0.25.

**Certified Reference Materials**
The reference compounds used for XANES and EXAFS analysis were obtained by procedures described in the literature [18,19].

**Samples Preparation of Ormosil Films**
**Chemicals Reagents**
Tetraethylorthosilicate (TEOS, 98%), 3-(glycidyloxypropyl) trimethoxysilane (GLYMO, 98%), and 4-(triethoxysilyl) butyronitrile (BUTS, 98%), Phosphotungstic Acid hydrate (PWA), Zinc Nitrate (Zn (NO3)2.6H2O), acetone 99.5% and ethanol 99.8% was supplied by QHEMIS (SP,30 Brazil).

**Ormosil Films containing Phosphotungstates doped with $TiO_2$**
the sol formulations used in the films preparation is reported in Table 1; all solutions were prepared in polypropylene beakers. The general procedure for all preparations was to add the silanes (TEOS, BUTS, GLYMO) to the beakers with a micropipette and then add 25 mL of solvent (ethanol/acetone 9:1) under magnetic stirring; immediately afterwards 25 mL of freshly prepared PWA solution in the mixture ethanol/acetone, which was added under magnetic stirring. The last step consisted in adding Titanium dioxide (TiO2) nanoparticles in suspension (0.1%m/v) with different concentrations with a micropipette. The mixture was left under magnetic stirring for 10 min before to be deposited on Silicon [111] substrates.

**Table 1: Sol formulations used in the preparation of ormosil films containing phosphotungstate doped with $TiO_2$ nanoparticles**

| Sample Code | [HPW] $10^{-3}$mol | [TEOS] $10^{-3}$mol | [GLYMO] $10^{-3}$mol | [BUTS] $10^{-3}$mol | Volume ($10^{-6}$L) $TiO_2$ nanoparticles suspension 0.1%. |
|---|---|---|---|---|---|
| SNP | 0.75 | 9 | 6.8 | 1.5 | "---" |
| A2 | 0.75 | 9 | 6.8 | 1.5 | $2.0.10^1$ |
| A6 | 0.75 | 9 | 6.8 | 1.5 | $2.0.10^2$ |
| A7 | 0.75 | 9 | 6.8 | 1.5 | $1.0.10^3$ |
| A8 | 0.75 | 9 | 6.8 | 1.5 | $2.0.10^3$ |

**Table 2: Nominal Titanium and Tungsten concentrations of ormosil films containing phosphotungstate doped with $TiO_2$ nanoparticles**

| Sample Code | Nominal Titanium Concentration [Ti] (%m/m) | Nominal Tungsten Concentration [W] (%m/m) |
|---|---|---|
| SNP | --- | 46.5 |
| A2 | $1.6.\ 10^{-2}$ | 46.5 |
| A6 | $1.6.\ 10^{-1}$ | 46.5 |
| A7 | 0.8 | 45.9 |
| A8 | 1.6 | 45.1 |

### Ormosil Films containing Phosphotungstates doped with $Zn^{2+}$ ions

the sol formulations of the prepared samples are summarized in Table 3. In the procedure of sol preparation, the alkoxysilanes (TEOS, GLYMO and BUTS) were dissolved in 25 mL of ethanol in a polypropylene beaker, followed by addition of 25 mL of freshly prepared PWA solution in ethanol under stirring. Then, ZnO suspension (0. 1mol.$L^{-1}$) in ethanol was added and the mixture was kept under magnetic stirring for 5 minutes in order to homogenize the sol. Finally, 825 µL of deionized water was added to this mixture and kept under stirring for more 10 minutes, before to be deposited on Silicon [111] substrates.

**Table 3: Sol Formulations used in the Preparation of Ormosil Films Containing Phosphotungstate Doped $Zn^{2+}$ ions [3]**

| Sample Code | [HPW] $10^{-3}$mol | [TEOS] $10^{-3}$mol | [GLYMO] $10^{-3}$mol | [BUTS] $10^{-3}$mol | ZnO $10^{-3}$mol |
|---|---|---|---|---|---|
| Z0.25 | 0.75 | 9 | 6.8 | 1.5 | 0.05 |
| Z0.5 | 0.75 | 9 | 6.8 | 1.5 | 0.1 |
| Z1.0 | 0.75 | 9 | 6.8 | 1.5 | 0.2 |

**Table 4: Nominal Zinc and Tungsten Concentrations of Ormosil films Containing Phosphotungstate Doped $Zn^{2+}$ ions**

| Sample Code | Nominal Zinc Concentration [Zn] (%m/m) | Nominal Tungsten Concentration [W] (%m/m) |
|---|---|---|
| 36E | --- | 46.5 |
| Z0.25 | $9.0.10^{-2}$ | 46.5 |
| Z0.50 | $1.8.10^{-1}$ | 46.5 |
| Z1.0 | $3.610^{-1}$ | 46.4 |

Solutions of Tungsten and Molybdenum compounds- the reagents used are summarized in Table 5.

**Table 5: Chemical Reagents used in the Experiments of Tungsten and Molybdenum Solutions [3]**

| Compound | Chemical Formula | Supplier |
|---|---|---|
| Phosphotungstic acid hydrated (reagent degree) | $H_3PW_{12}O_{40}.XH_2O$(HPW) | SIGMA-ALDRICH |
| Phosphomolybdic acid hydrated (reagent degree) | $H_3PMo_{12}O_{40}.XH_2O$(HPMo) | SIGMA-ALDRICH |
| Sodium Tungstate Di-hydrated (≥99%) | $Na_2WO_4.2H_2O$ | FLUKA |
| Sodium Molybdate Di-hydrated (≥99.5) | $Na_2MoO_4.2H_2O$ | SIGMA-ALDRICH |
| Ammonium Paratungstate (> 99%) | $[(NH_4)_{10}(H_2W_{12}O_{42})\cdot 10H_2O$ | SIGMA-ALDRICH |
| Phosphoric acid (85 % m/m) | $H_3PO_4$ | SIGMA-ALDRICH |

### Solutions of Certified Reference Materials for Phosphorous and Tungsten

We prepared Phosphorous and Tungsten solutions from standard solutions of 1000 mg/Kg TraceCERT® for ICP-OES analyses of these elements.

## Results

### XRF

### EDXRF Analyses

### Ormosil Films containing Phosphotungstates Doped with $TiO_2$

The Figure 1 shows the Phosphorous and Tungsten concentration (% m/m), obtained by XRF, in ormosil films containing phosphotungstates.

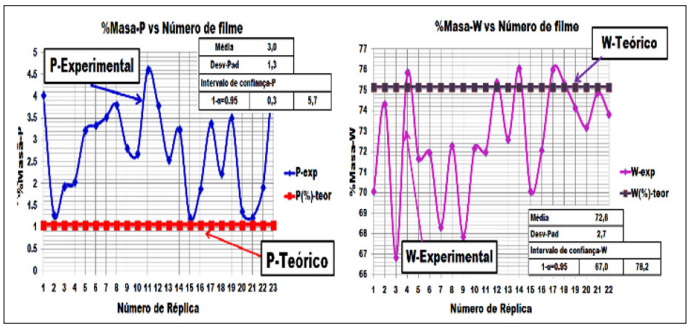


**Figure 1:** Phosphorous and Tungsten concentration in ormosil films [3]

The Figure 1 shows that the concentration of Phosphorous was overestimated and the concentration of Tungsten has been underestimated.

### Ormosil Films containing Phosphotungstates Doped with $Zn^{2+}$ ions

The figure 2 shows the variation of Phosphorous concentration (% diminution), obtained by XRF, as function of the Zinc concentration in ormosil films containing phosphotungstates doped with $Zn^{2+}$ ions.

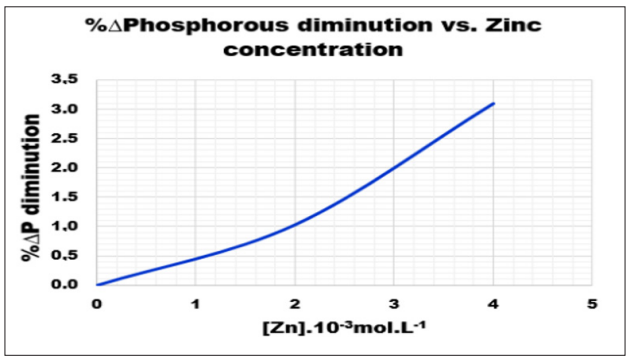


**Figure 2:** Phosphorous diminution (in %) as function of Zinc concentration in ormosil films

This figure reveals that in the extent that the Zinc concentration in ormosil films increases, the enhancement in Phosphorous concentration, as was reported by Elguera Ysnaga, undergoes a diminution [3]. In order to clarify these effects, were performed a series of experiments with Tungsten and Molybdenum compounds (in solutions and pellets):

**Experiment A-Solutions of Certified Reference Materials for Phosphorous and Tungsten**

The figure 3 shows the Tungsten concentrations obtained by XRF as function of the moles ratio of Phosphorous and Tungsten (P/W), correspondent to the solutions prepared from ICP-OES standard solutions of these elements.

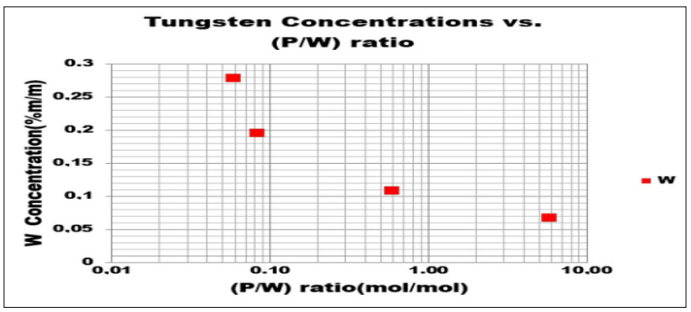


**Figure 3:** Tungsten concentrations obtained by EDXRF as function of Phosphorous/Tungsten moles ratio in the mixtures of standard solutions for Phosphorous and Tungsten

From this Figure, it can be seen that in the extent of the content of Phosphorous increases, the Tungsten concentrations undergo a diminution, but this is not the same magnitude than it was observed for the mol ratio (P/W) existent in the ormosil films (1/12).

**Experiment B-Solutions of Phosphoric Acid and Sodium Tungstate**

For this experiment, we prepared aqueous solutions of Sodium tungstate di-hydrated ($Na_2WO_4.2H_2O$) with the following concentrations of Tungsten: 50, 100, 200 and 400.$10^{-3}$mol.$L^{-1}$(mmol), to which were added different volumes of a phosphoric acid ($H_3PO_4$) solution with concentration 0.17 mol.$L^{-1}$. These measurements were performed at the Minipal4 EDXRF spectrometer, obtaining the following results (4 repetitions per experimental point):

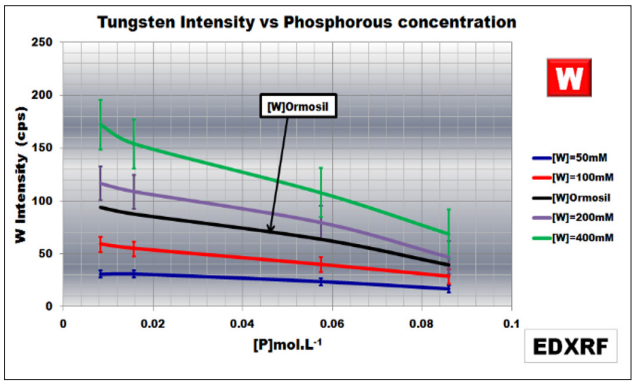


**Figure 4:** XRF Tungsten intensities (W-Lα line) as function of Phosphorous concentration in the mixtures of Sodium Tungstate ($Na_2WO_4$) and Phosphoric acid ($H_3PO_4$) solutions

This Figure reveals that at higher Phosphorous concentrations, the more concentrated Tungsten solutions undergo an important decrement in their correspondent W intensities.

Taking into account the volume of the preparation (50.$10^{-3}$L) and the mass of phosphotungstic acid ($H_3PW_{12}O_{40}$) used (2.25 grams) in the preparation of ormosil films [Ref. 2, 3]; the correspondent concentration of Phosphorous in the colloidal suspension was about 0.014 mol. $L^{-1}$. It is shown in the next Figure the correlation between the mol ratio of Phosphorous and Tungsten present (P/W) with the Tungsten concentrations ratio [W]/[$W_0$], being [W] and [$W_0$] the experimental and theoretical values respectively:

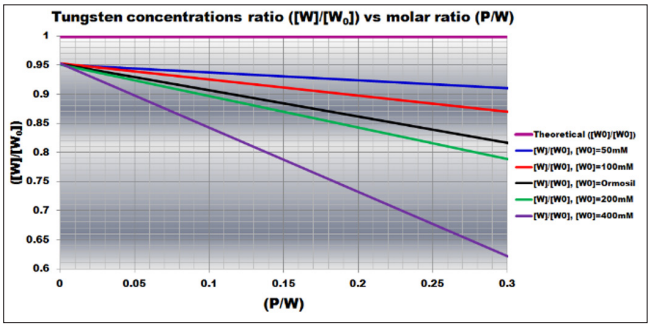


**Figure 5:** Correlation between experimental and nominal Tungsten concentrations ([W]/[$W_0$]) and the molar ratio (P/W) in the mixtures of Sodium Tungstate ($Na_2WO_4$) and Phosphoric acid ($H_3PO_4$) solutions

Evaluating the correlations obtained at the moles ratio present in phosphotungstates (P/W = 1/12 = 0.083) contained within ormosil samples:

- When the theoretical Tungsten concentration increases from 50.$10^{-3}$mol.$L^{-1}$ (50mM, blue line) to 100.$10^{-3}$mol.$L^{-1}$ (100mM, red line), the Tungsten concentrations ratio ([W]/[$W_0$]) do not diminish in significantly form.
- When the theoretical Tungsten concentrations are 166.$10^{-3}$mol.$L^{-1}$ (166mM, black line) and 200.$10^{-3}$mol.$L^{-1}$ (200 mM, green line), one realizes the slight influence of Phosphorous moles.
- At Tungsten concentrations about 400.$10^{-3}$mol.$L^{-1}$ (400 mM, violet line), there is a marked influence (interference) of Phosphorous moles in the Tungsten experimental concentration. Thus, the Tungsten fluorescence intensity will experience a diminution (due to self-absorption by Phosphorous), resulting in the decrease of its concentration determined by XRF.

**Experiment C-Solutions of Phosphoric Acid and Sodium Molybdate**

In this experiment, we prepared aqueous solutions of Sodium molybdate di-hydrated ($Na_2MoO_4.2H_2O$) with the following concentrations of Molybdenum: 50, 100, 200 and 400.$10^{-3}$mol.$L^{-1}$, to which were added different volumes of a phosphoric acid ($H_3PO_4$) solution with concentration 0.17 mol.$L^{-1}$, obtaining the following results (4 repetitions per experimental point)

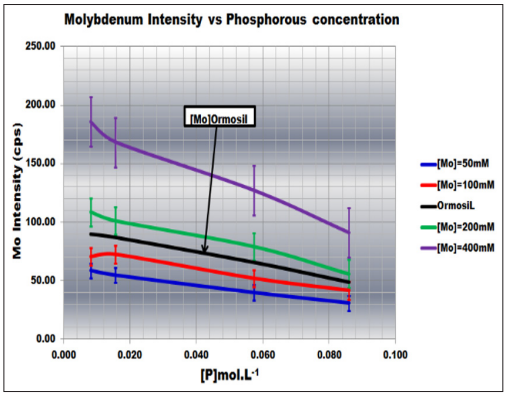


**Figure 6:** XRF Molybdenum intensities (Mo-Kα line) as function of Phosphorous concentration in the mixtures of Sodium Molybdate ($Na_2MoO_4$) and Phosphoric acid ($H_3PO_4$) solutions

This Figure reveals that the Molybdenum intensities exhibit similar tendency as the Tungsten ones, but with a marked difference at concentration $400.10^{-3}$mol.L$^{-1}$. In the next Figure we show the correlation between the mol ratio of Phosphorous and Molybdenum present (P/Mo) with the Molybdenum concentrations ratio [Mo]/[$Mo_0$], being [Mo] and [$Mo_0$] the experimental and theoretical values respectively:

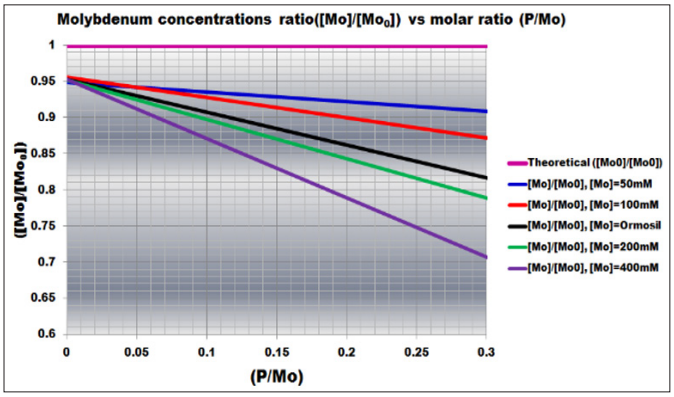


**Figure 7:** Correlation between experimental and nominal Molybdenum concentrations ([Mo]/[$Mo_0$]) and the molar ratio (Mo/P) in the mixtures of Sodium Tungstate ($Na_2MoO_4$) and Phosphoric acid ($H_3PO_4$) solutions

Evaluating the correlations obtained at the mol ratio present in phosphomolybdates (P/Mo = 1/12 = 0.083), we obtain the same tendency than for the Tungsten: that for Molybdenum concentrations around of $400.10^{-3}$mol.L$^{-1}$ (400 mM, violet line), there is a marked influence (interference) of Phosphorous moles. The similar tendency obtained from the experiments with Tungsten and Molybdenum solutions are resumed and illustrated in the next Figure:

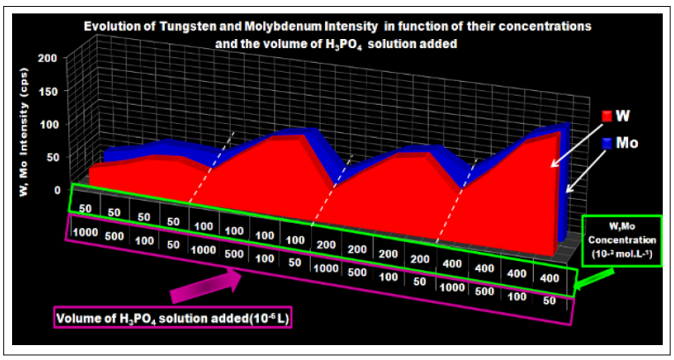


**Figure 8:** Evolution of Tungsten (W-Lα line- red) and Molybdenum (Mo-Kα line-blue) XRF intensities as function of concentration and the volume of $H_3PO_4$ added

**Experiment D- Solutions of Phosphotungstic Acid and Ammonium Paratungstate**

For this experiment were prepared, in separated form, aqueous solutions of Phosphotungstic acid ($H_3PW_{12}O_{40}$. $21H_2O$, 67.6%m/m of W) and Ammonium paratungstate ($[(NH_4)_{10}(H_2W_{12}O_{42})$ $\bullet 10H_2O)]$, 68.08%m/m of W). The concentration of both solutions was 10g/L (the reagents were used without previous drying). The measurements were performed at Minipal4-PANalytical EDXRF spectrometer, obtaining the following results (10 repetitions per measurement):

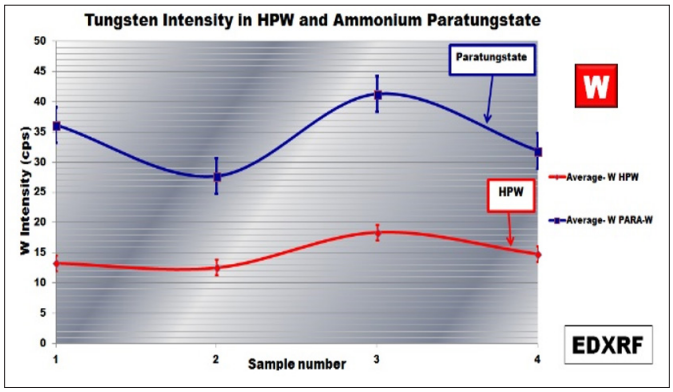


**Figure 9:** Tungsten XRF intensities (W-Lα line) for Phosphotungstic acid (red-line) and Ammonium Paratungstate (blue-line)

**Experiment E- Pellets of Phosphotungstic Acid and Ammonium Paratungstate**

For this experiment were made 2 pellets, prepared from 1 g of Phosphotungstic acid ($H_3PW_{12}O_{40}.6H_2O$, 69.09%m/m of W) diluted with 3g of Boric acid and 1g of Ammonium paratungstate ($[(NH_4)_{10}$ $(H_2W_{12}O_{42})$ $\bullet 10H_2O)]$, 70.43%m/m of W) diluted with 3 g Boric Acid (the reagents were previously dried). The measurements were performed at Rigaku NEX-CG EDXRF spectrometer, obtaining the following results:

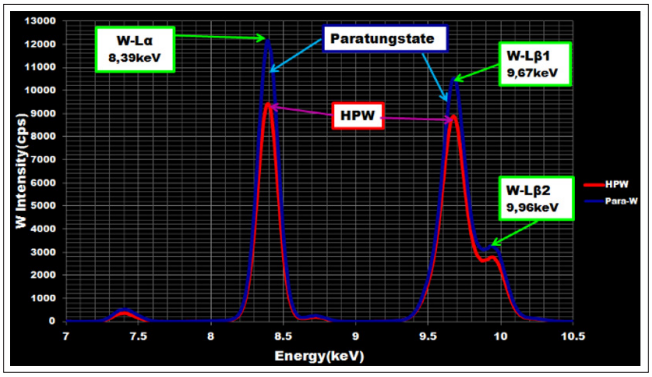


**Figure 10:** Tungsten Spectra for Phosphotungstic acid (red) and Ammonium Paratungstate (blue)

From the results of the experiments D and E, it can be inferred that in similar concentrations ranges, the Tungsten intensity from the paratungstates is higher than the intensity from the phosphotungstates. From these results, we have evidence of the interference of Phosphorous on the Tungsten fluorescence in phosphotungstate structure, because the two compounds are polyoxoanions with similar structures, but the paratungstate has no Phosphorous in its center of symmetry in opposition to the phosphotungstates.

The results presented in the experiments A, B, C, D and E were referring to the X-ray fluorescence in energy dispersive mode (EDXRF), wherein the energy resolution (0.2keV) can sometimes limit the analysis of existing interference in a given matrix. At low energy resolution, it is not possible to resolve the overlapping lines on the XRF spectrum. Therefore, were performed analyses based on X-ray fluorescence in the wavelength dispersive mode (WDXRF), usually with higher resolution than EDXRF.

**WDXRF Analyses**

The WDXRF measurements were performed in ormosil films, deposited by Drop-Casting on Mylar® substrates of thickness 3.6μm, at RIX-3000-Rigaku WDXRF spectrometer with crystal LiF analyzer (220), which spectrum is shown in the next Figure:

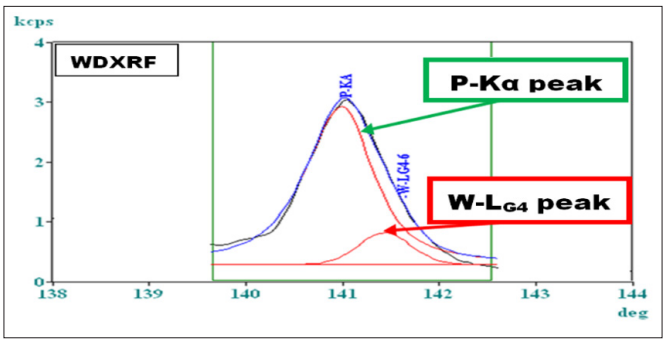


**Figure 11:** WDXRF spectrum of ormosil film showing the interference between Phosphorous and Tungsten peaks

From this Figure, we can see that there is a superposition of Tungsten line W-$L_{G4}$ with the Phosphorous line P-Kα. The W-$L_{G4}$ line is a fourth order reflection line (having 0.1% of the intensity of the main line W-Lα), which can be viewed only in analyses by WDXRF.

**XANES and EXAFS**

**XANES**

The Figures 12 and 13 present the XANES spectra at W-LIII edge of Tungsten, for ormosil samples doped with $Zn^{2+}$ and $Ca^{2+}$ cations, using as reference compounds $H_3PW_{12}O_{40}$ (namely PWA), $ZnWO_4$ and $CaWO_4$.

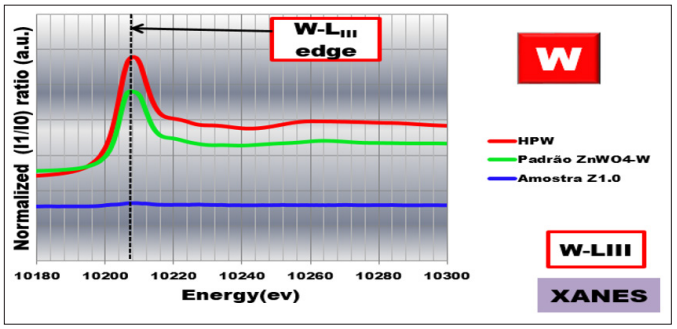


**Figure 12:** XANES spectra at W-$L_{III}$ edge of ormosil samples doped with $Zn^{2+}$ cations

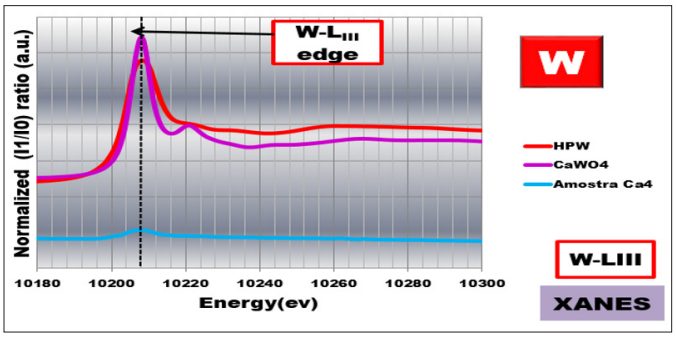


**Figure 13:** XANES spectra at W-$L_{III}$ edge of ormosil samples doped with $Ca^{2+}$ cations

These Figures reveal no important differences at the pre-edge and edge regions (ranging from 10180 to 10210 eV) for Tungsten. The post-edge region (ranging from 10210 to 10300 eV) show differences between the samples and reference compounds used. The differences between $ZnWO_4$ and $CaWO_4$ at about 10220eV are based on their geometries. For $ZnWO_4$ is octahedral, for $CaWO_4$ tetrahedral, and for PWA octahedral distorted.

The Figures 14 and 15 present the XANES spectra at Zn-K and Ca-K edges of ormosil samples doped with $Zn^{2+}$ and $Ca^{2+}$ cations, using as reference compounds ZnO, $ZnNO_3.6H_2O$, $Zn_2SiO_4$ and $ZnWO_4$ for Zinc, and $CaCO_3$, $Ca_2SiO_4$ and $CaWO_4$ for Calcium.

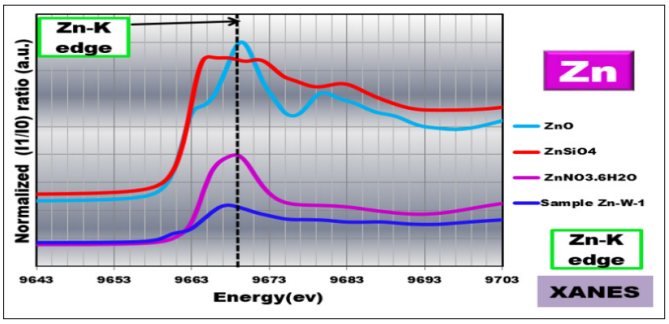


**Figure 14:** XANES spectra at Zn-K edge of ormosil samples doped with $Zn^{2+}$ cations and reference compounds

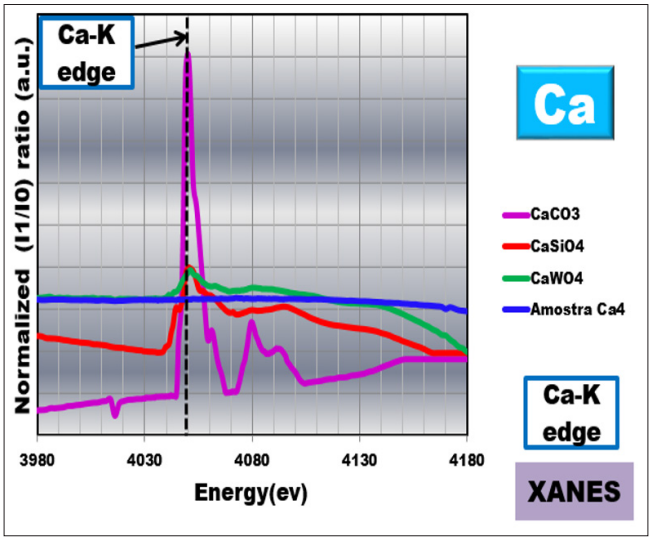


**Figure 15:** XANES spectra at Ca-K edge of ormosil samples doped with $Ca^{2+}$ cations

The Figure 14 reveals that at the pre-edge and edge regions, the ormosil sample doped with $Zn^{2+}$ cations resemble a combination of ZnO, $ZnNO_3.6H_2O$, $Zn_2SiO_4$ and $ZnWO_4$. At post-edge region (range 9673-9703 eV), the ormosil sample resembles more with $ZnNO_3.6H_2O$ than the other reference compounds. For the ormosil sample doped with $Ca^{2+}$ cations, illustrated in the Figure 15, it is difficult visualize in the pre-edge and edge regions, but the post-edge region resembles more a combination of $Ca_2SiO_4$ and $CaWO_4$ than $CaCO_3$.

**EXAFS**

**EXAFS of Tungsten Species**

In the Figures 16-21 we show the EXAFS signals and Fourier Transform at the W-$L_{III}$ edge of Tungsten for ormosil samples doped with $Zn^{2+}$ and $Ca^{2+}$ cations using as reference compounds $H_3PW_{12}O_{40}$, $ZnWO_4$ and $CaWO_4$ .

**For $H_3PW_{12}O_{40}$, $ZnWO_4$ and Ormosil Sample Doped with $Zn^{2+}$**

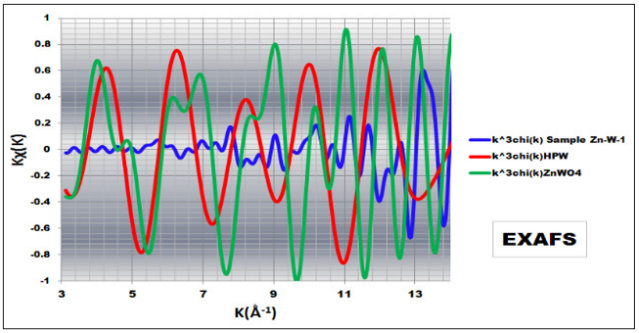


**Figure 16:** EXAFS signals at the W-$L_{III}$-edge of Tungsten for ormosil sample (blue line), $H_3PW_{12}O_{40}$ (red line) and $ZnWO_4$ (green line)

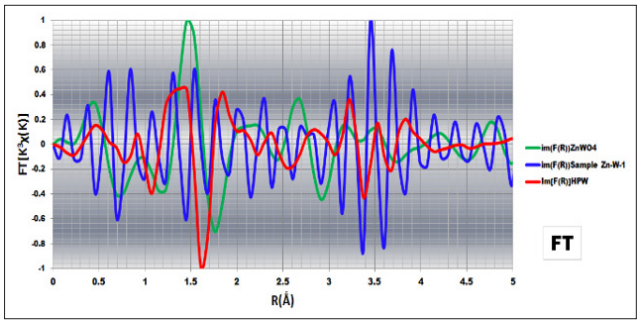


**Figure 17:** Fourier Transform at the W-$L_{III}$-edge of Tungsten for ormosil sample (blue line), $H_3PW_{12}O_{40}$ (red line) and $ZnWO_4$ (green line)

**For $H_3PW_{12}O_{40}$, $CaWO_4$ and Ormosil Sample Doped with $Ca^{2+}$**

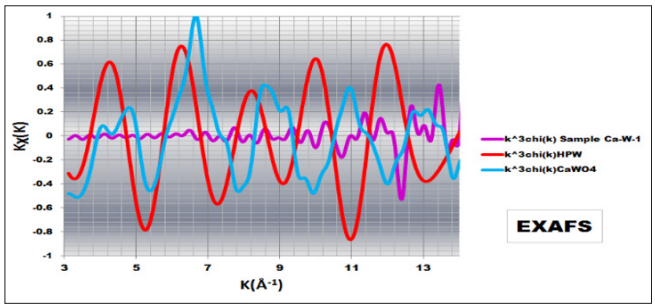


**Figure 18:** EXAFS signals at the W-$L_{III}$-edge of Tungsten for ormosil sample (purple line), $H_3PW_{12}O_{40}$ (red line) and $CaWO_4$ (light blue line).

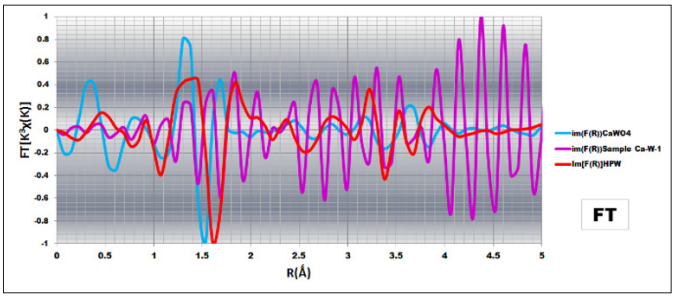


**Figure 19:** Fourier Transform at the W-$L_{III}$-edge of Tungsten for ormosil sample (purple line), $H_3PW_{12}O_{40}$ (red line) and $CaWO_4$ (light blue line)

**For Ormosil Samples Doped with $Zn^{2+}$and $Ca^{2+}$**

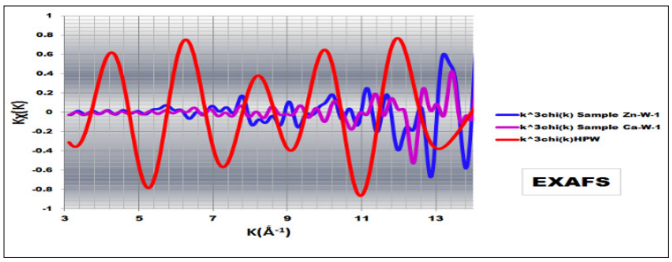


**Figure 20:** EXAFS signals at the W-$L_{III}$-edge of Tungsten for ormosil sample doped with $Zn^{2+}$ cations (blue line), ormosil sample doped with $Ca^{2+}$ cations (purple line), and $H_3PW_{12}O_{40}$ (red line)

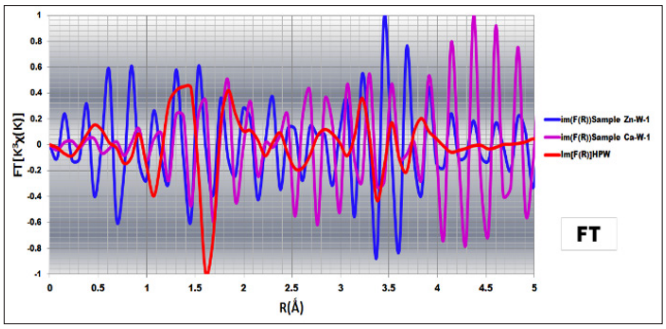


**Figure 21:** Fourier Transform at the W-$L_{III}$-edge of Tungsten for ormosil sample doped with $Zn^{2+}$ cations (blue line), ormosil sample doped with $Ca^{2+}$ cations (purple line), and $H_3PW_{12}O_{40}$ (red line)

From the Figure 16, 18 and 20, we observed that the EXAFS Tungsten signals correspondent to the ormosil samples doped with $Zn^{2+}$ and $Ca^{2+}$ cations resemble more to $ZnWO_4$ and $CaWO_4$ than $H_3PW_{12}O_{40}$. The Figures 17, 19 and 21, which show the Fourier Transform, reveal that at region between 0.3-1.2Å there are peaks correspondent to the ormosil samples that no appear in the reference compounds. From 1.3 to 4.0Å the samples exhibit peaks that resemble to $H_3PW_{12}O_{40}$, $ZnWO_4$ and $CaWO_4$. For values greater than 4.0Å, the samples present peaks that are more similar with $ZnWO_4$ and $CaWO_4$ than with PWA. The Figure 21 shows that the samples doped with $Zn^{2+}$ and $Ca^{2+}$ cations exhibit similar shape (except in the range for R< 1.0 Å) but differ in their intensities. From these observations, we can infer that in the region of EXAFS analysis there is/are other(s) type(s) of Tungsten specie (s) besides of the reference compounds used.

**EXAFS of Zinc Species**

In the Figures 22-29 we show the EXAFS signals and Fourier Transform at the Zn-K edge of ormosil samples doped with $Zn^{2+}$ cations using as reference compounds ZnO, $ZnNO_3.6H_2O$, $Zn_2SiO_4$ and $ZnWO_4$.

### For ZnO and Ormosil Sample Doped with $Zn^{2+}$

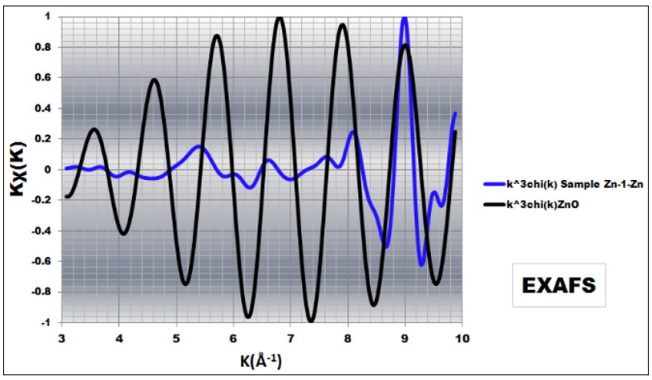


**Figure 22:** EXAFS signals at the Zn-K-edge of Zinc for ormosil sample doped with $Zn^{2+}$ cations (blue line), and ZnO (black line)

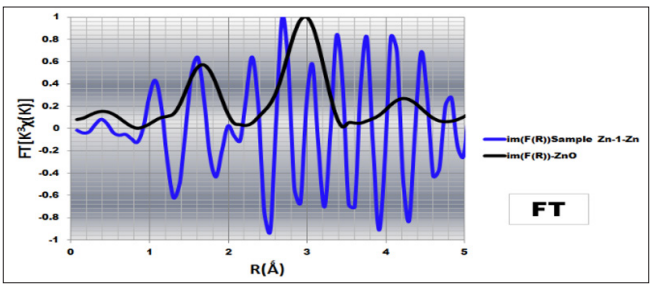


**Figure 23:** Fourier Transform at the Zn-K-edge of Zinc for ormosil sample doped with $Zn^{2+}$ cations (blue line), and ZnO (black line)

### For $ZnNO_3.6H_2O$ and Ormosil Sample Doped with $Zn^{2+}$

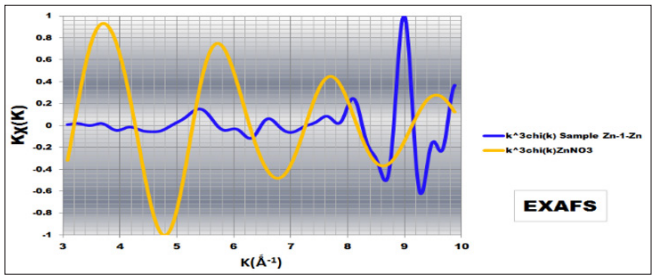


**Figure 24:** EXAFS signals at the Zn-K-edge of Zinc for ormosil sample doped with $Zn^{2+}$ cations (blue line), and $ZnNO_3.6H_2O$ (orange line)

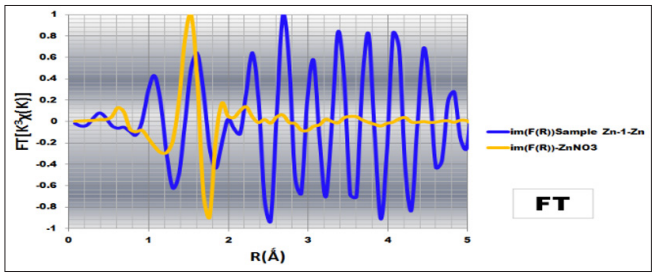


**Figure 25:** Fourier Transform at the Zn-K-edge of Zinc for ormosil sample doped with $Zn^{2+}$ cations (blue line), and $ZnNO_3.6H_2O$ (orange line)

### For $Zn_2SiO_4$ and Ormosil Sample Doped with $Zn^{2+}$

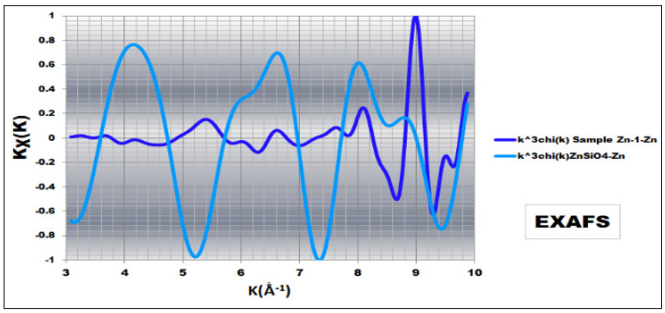


**Figure 26:** EXAFS signals at the Zn-K-edge of Zinc for ormosil sample doped with $Zn^{2+}$ cations (blue line), and $Zn_2SiO_4$ (light blue line)

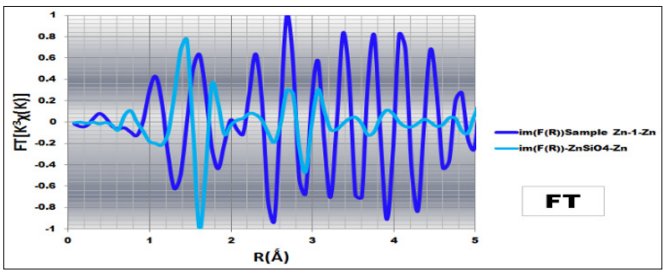


**Figure 27:** Fourier Transform at the Zn-K-edge of Zinc for ormosil sample doped with $Zn^{2+}$ cations (blue line), and $Zn_2SiO_4$ (light blue line).

### ZnWO4 and Ormosil Sample Doped with Zn2+

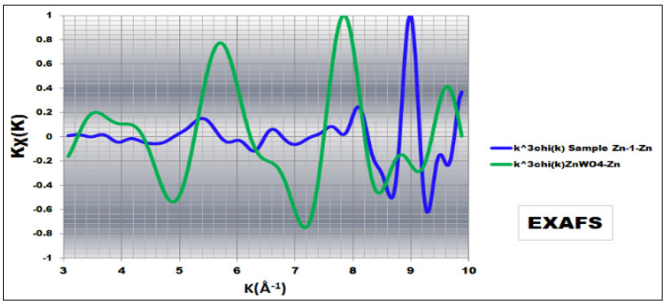


**Figure 28:** EXAFS signals at the Zn-K-edge of Zinc for ormosil sample doped with $Zn^{2+}$ cations (blue line), and $ZnWO_4$ (green line).

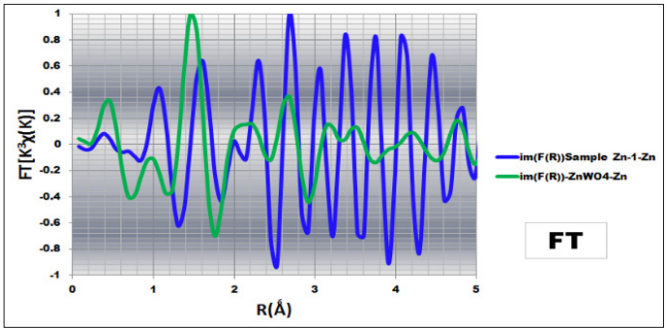


**Figure 29:** Fourier Transform at the Zn-K-edge of Zinc for ormosil sample doped with $Zn^{2+}$ cations (blue line), and $ZnWO_4$ (green line)

The EXAFS Zinc signals correspondent to the ormosil samples doped with $Zn^{2+}$ cations (Figures 22, 24, 26 and 28), resemble more to $ZnWO_4$ and ZnO (K vector values less than 8.0Å-1). The Fourier Transform (Figures 23, 25, 27 and 29), reveal that at region between 0.3-1.2Å there are peaks correspondent to the ormosil samples that no appear in the reference compounds; from 0.3 to 2.0Å (first coordination shell), the ormosil sample exhibit peaks that resemble to a combination of ZnO, $ZnNO_3.6H_2O$ and $ZnWO_4$. For values greater than 2.0Å, the ormosil sample present similar peaks that $ZnWO_4$ and $Zn_2SiO_4$.From this later observation, we can infer that in the ormosil sample outer of the first coordination shell is possible the presence of Tungsten and Silicon close to Zinc.

In order to deduce what other(s) specie(s) of Tungsten and Zinc are present, in the Tables 6 and 7 we make a comparison between the distances obtained from Fourier Transform, from EXAFS measurements, and the correspondent values from DRX tables:

**Table 6: Comparison between distances obtained by FT-EXAFS and DRX for ormosil samples and reference compounds in Tungsten measurements**

| Distance Sample Zn-1-W FT-EXAFS | Distance Sample Ca-1-W FT-EXAFS | Distance HPW FT-EXAFS | Distance HPW* DRX Values | Distance HSiW* DRX Values | Distance $ZnWO_4$ FT-EXAFS | Distance $CaWO_4$ FT-EXAFS | Distance $ZnWO_4$ DRX Values | Distance W DRX Values |
|---|---|---|---|---|---|---|---|---|
| 0.15Å | 0.15Å | 0.07Å | --------- | --------- | 0.07Å | 0.07Å | --------- | --------- |
| 0.23 | 0.23 | 0.15 | --------- | --------- | 0.15 | --------- | --------- | --------- |
| 0.31 | 0.38 | 0.46 | --------- | --------- | 0.46 | 0.38 | --------- | --------- |
| 0.46 | 0.53 | --------- | --------- | --------- | --------- | 0.53 | --------- | --------- |
| 0.61 | 0.61 | 0.61 | --------- | --------- | --------- | 0.61 | --------- | --------- |
| 0.69 | 0.77 | --------- | 0.79Å | --------- | 0.77 | 0.77 | --------- | 0.79Å |
| 0.77 | 0.92 | 0.92 | 0.91 | --------- | 0.92 | 0.84 | --------- | 0.91 |
| 1.0 | 1.15 | --------- | --------- | --------- | --------- | --------- | --------- | 1.0 |
| 1.23 | 1.22 | --------- | --------- | --------- | 1.22 | 1.30 | --------- | 1.29 |
| 1.45 | 1.38 | 1.45 | --------- | --------- | 1.45 | --------- | 1.45Å | --------- |
| 1.53 | 1.45 | 1.53 | 1.53 | 1.53Å | --------- | 1.53 | --------- | --------- |
| 1.69 | 1.61 | --------- | --------- | --------- | --------- | 1.61 | --------- | 1.58 |
| 1.76 | 1.84 | 1.76 | 1.70 | 1.72 | 1.76 | --------- | 1.77 | --------- |
| 1.92 | 1.91 | --------- | 1.91 | --------- | --------- | --------- | --------- | --------- |
| 1.99 | 1.99 | 1.99 | --------- | 1.97 | --------- | --------- | --------- | --------- |
| 2.14 | 2.14 | --------- | --------- | --------- | 2.14 | 2.07 | 2.18 | --------- |
| 2.30 | 2.22 | 2.22 | 2.23 | 2.22 | --------- | --------- | --------- | 2.24 |
| 2.38 | 2.45 | 2.37 | 2.43 | 2.38 | 2.37 | 2.45 | 2.44 | --------- |
| 2.53 | 2.52 | 2.53 | 2.50 | 2.58 | --------- | 2.60 | --------- | --------- |
| 2.60 | 2.68 | --------- | --------- | --------- | --------- | --------- | --------- | --------- |
| 2.68 | 2.76 | --------- | 2.70 | --------- | 2.68 | 2.76 | --------- | --------- |
| 2.72 | 2.84 | 2.83 | 2.83 | 2.88 | --------- | --------- | --------- | --------- |
| 2.76 | --------- | --------- | --------- | --------- | --------- | --------- | --------- | --------- |
| 2.91 | 2.99 | --------- | 2.98 | --------- | 2.91 | 2.99 | 2.91 | --------- |
| 3.07 | 3.07 | --------- | --------- | --------- | --------- | --------- | --------- | --------- |
| 3.14 | 3.14 | 3.14 | 3.13 | 3.04 | 3.14 | 3.14 | --------- | --------- |
| --------- | 3.22 | 3.22 | 3.21 | 3.20 | --------- | --------- | --------- | --------- |
| --------- | 3.29 | --------- | 3.32 | --------- | --------- | --------- | --------- | --------- |
| 3.37 | 3.37 | 3.45 | 3.40 | 3.52 | 3.45 | 3.37 | --------- | --------- |
| --------- | 3.45 | --------- | --------- | --------- | --------- | --------- | --------- | --------- |
| 3.60 | 3.68 | 3.68 | 3.60 | --------- | 3.68 | 3.60 | 3.62 | --------- |
| 3.68 | 3.75 | --------- | --------- | --------- | --------- | --------- | --------- | --------- |
| 3.83 | 3.83 | --------- | --------- | --------- | --------- | 3.83 | --------- | --------- |
| 3.91 | 3.91 | 3.83 | 3.89 | 3.90 | --------- | --------- | --------- | --------- |
| 3.99 | 3.98 | --------- | --------- | --------- | --------- | 3.99 | --------- | --------- |
| 4.07 | 4.07 | --------- | --------- | --------- | --------- | --------- | --------- | --------- |
| 4.14 | 4.14 | --------- | --------- | --------- | 4.21 | 4.14 | --------- | --------- |
| 4.30 | 4.30 | --------- | --------- | --------- | --------- | --------- | --------- | --------- |
| 4.37 | 4.37 | 4.37 | --------- | 4.32 | --------- | 4.37 | --------- | --------- |
| 4.52 | 4.52 | --------- | --------- | --------- | 4.52 | --------- | --------- | --------- |
| 4.60 | 4.60 | --------- | --------- | --------- | --------- | 4.60 | --------- | --------- |
| 4.75 | 4.75 | --------- | 4.74 | --------- | 4.75 | --------- | 4.70 | --------- |
| 4.83 | 4.90 | --------- | --------- | 4.90 | 4.90 | 4.83 | --------- | --------- |

*HPW and HSiW are abbreviations correspond to the compounds $H_3PW_{12}O_{40}$ and $H_4SiW_{12}O_{40}$ respectively.

**Table 7: Comparison between distances obtained by FT-EXAFS and DRX for ormosil samples and reference compounds in Zinc measurements**

| Distance Sample Zn-1-Zn FT-EXAFS | Distance $ZnWO_4$ FT-EXAFS | Distance $ZnWO_4$ DRX Values | Distance $Zn_2SiO_4$ FT-EXAFS | Distance $Zn_2SiO_4$ DRX Values | Distance ZnO FT-EXAFS | Distance ZnO DRX Values | Distance $ZnNO_3$ FT-EXAFS | Distance $ZnNO_3$ DRX Values | Distance Zn DRX Values |
|---|---|---|---|---|---|---|---|---|---|
| 0.38Å | 0.46Å | --------- | --------- | --------- | 0.38Å | --------- | --------- | --------- | --------- |
| 1.07 | 0.99 | --------- | --------- | --------- | --------- | --------- | --------- | --------- | 1.09Å |
| 1.30 | --------- | --------- | 1.15Å | --------- | --------- | --------- | 1.22Å | --------- | 1.34 |
| 1.53 | 1.46 | 1.47Å | 1.46 | 1.49Å | --------- | --------- | 1.46 | --------- | --------- |
| 1.61 | --------- | --------- | 1.61 | 1.64 | --------- | --------- | --------- | --------- | --------- |
| 1.84 | 1.76 | 1.77 | 1.69 | 1.69 | 1.68 | 1.81Å | 1.69 | --------- | 1.69 |
| 1.99 | 2.07 | 2.05 | 1.91 | 1.95 | --------- | --------- | 1.91 | --------- | --------- |
| 2.14 | --------- | --------- | --------- | --------- | --------- | --------- | --------- | --------- | 2.09 |
| 2.30 | --------- | --------- | 2.22 | 2.25 | --------- | --------- | 2.22 | --------- | 2.31 |
| 2.53 | 2.45 | 2.46 | 2.53 | 2.54 | --------- | 2.48 | --------- | --------- | 2.47 |
| 2.60 | 2.68 | --------- | 2.76 | 2.72 | --------- | 2.60 | 2.68 | 2.76Å | --------- |
| 2.91 | 2.91 | 2.91 | 2.91 | 2.85 | 2.82 | --------- | --------- | --------- | --------- |
| 2.99 | --------- | 2.93 | 2.99 | 3.10 | 2.99 | --------- | --------- | --------- | --------- |
| 3.22 | 3.22 | --------- | 3.22 | 3.24 | --------- | 3.21 | 3.22 | 3.22 | --------- |
| 3.37 | 3.29 | --------- | 3.52 | 3.51 | --------- | 3.60 | --------- | --------- | --------- |
| 3.52 | 3.52 | 3.62 | 3.68 | 3.71 | --------- | --------- | --------- | --------- | --------- |
| 3.78 | --------- | --------- | --------- | --------- | --------- | --------- | --------- | --------- | --------- |
| 3.91 | --------- | --------- | --------- | --------- | --------- | --------- | --------- | --------- | --------- |
| 4.07 | --------- | --------- | 4.0 | 4.05 | --------- | --------- | --------- | --------- | --------- |
| 4.29 | 4.21 | --------- | --------- | --------- | --------- | --------- | 4.21 | 4.19 | --------- |
| 4.45 | --------- | --------- | 4.37 | 4.40 | 4.29 | --------- | --------- | --------- | --------- |
| 4.60 | 4.52 | --------- | --------- | --------- | --------- | --------- | --------- | --------- | --------- |
| 4.83 | 4.75 | 4.69 | 4.67 | --------- | 4.75 | --------- | --------- | --------- | --------- |

| Distance Sample Zn-1-Zn FT-EXAFS | Distance $ZnCO_3$-$Zn(OH)_2$ FT-EXAFS |
|---|---|
| 1.07 Å | 0.99 Å |
| 1.53 | 1.46 |
| 1.61 | 1.69 |
| 1.99 | 1.99 |
| 2.30 | 2.37 |
| 2.60 | 2.60 |
| 2.91 | 2.83 |
| 2.99 | 2.99 |
| 3.22 | 3.22 |
| 3.37 | 3.37 |
| 3.52 | 3.52 |
| 3.78 | 3.78 |
| 3.91 | 3.91 |
| 4.07 | 4.07 |
| 4.29 | 4.21 |
| 4.45 | 4.37 |
| 4.60 | 4.67 |
| 4.83 | 4.90 |

From the Table 6, we can see that in the region of 1.0-1.2Å, the samples exhibit similar distances that the Tungsten elemental obtained by DRX; for other regions the ormosil sample exhibit similar distances with $ZnWO_4$ and $CaWO_4$. The Table 7 shows that ormosil sample in the region of 1.0-1.2Å present similar distances that Zinc elemental obtained by DRX.

**Hypotheses Proposed**

The following model represents the partial absorption of photons emitted by Tungsten cations ($W^{6+}$), in order to generate X-ray emission processes in the other constituent elements within the ormosil matrix. However, as EDXRF detects only from Sodium (Z=11), the elements which is possible observe this effect are Silicon (Si) and Phosphorous (P). The experimental results showed the effect of self-absorption of radiation emitted by the Tungsten (W), particularly by Phosphorus (P), generating Secondary Fluorescence (radiative mechanism) of the latter element. Our hypothesis is based on that these elements (P, W) are present as constituents of the same molecule: the phosphotungstate ($[PW_{12}O_{40}]^{-3}$), which does not change its structure in significant form after the sol-gel process [1,2]. In the next Figure shows schematically this hypothesis:

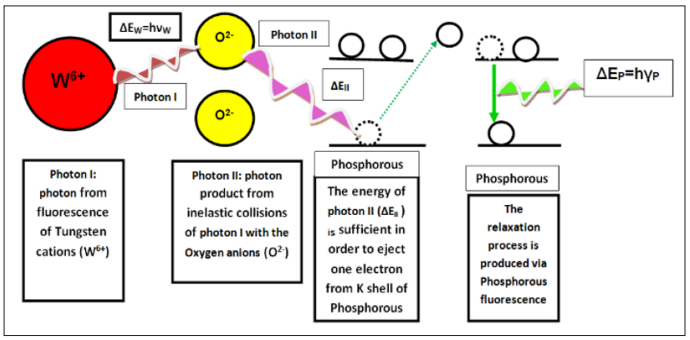


**Figure 30:** Proposed scheme of secondary fluorescence of Phosphorous in H3PW12O40

Nevertheless, as the Phosphorus is a light element (Z = 15), will be more likely that it undergoes decay via Auger effect (non-radiative mechanism), which is shown in the model illustrated in Figure 31:

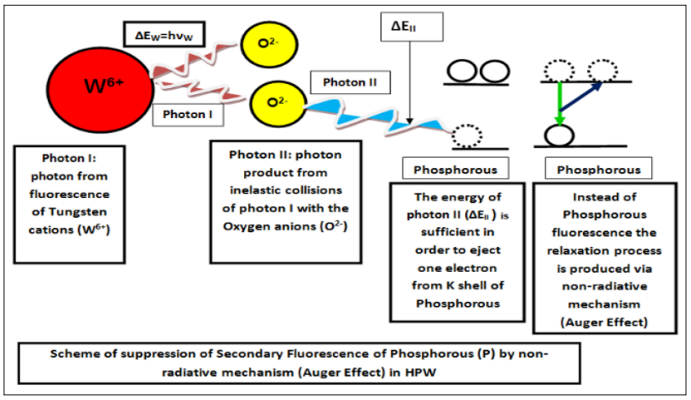


**Figure 31:** Proposed scheme of Auger effect of Phosphorous in H3PW12O40

For the Phosphorous, the Auger yield is 93.7%, being much higher than its correspondent X-Ray Fluorescence yield (6.3%).

In the scheme shown in Figure 30, our hypothesis of the secondary fluorescence of Phosphorous in the phosphotungstates is based on in the inelastic collisions between the X-ray photons, from the Tungsten cations ($W^{6+}$), with the Oxygen anions ($O^{2-}$). The probability of these collisions is greater when the elements involved have a lower atomic number (Z), and can becomes significant if it is taken into consideration that the amount of $O^{2-}$ present in the structure of phosphotungstates. However, only the hypothesis of secondary X-ray fluorescence is not sufficient in order to support the artificial increase in the Phosphorous concentration. For this reason, other phenomena have to be considered, for example the X-Ray Resonant Raman Scattering (XRRS). This scattering is important in light elements and if they are close in atomic number. As the ormosil contains Carbon (Z = 6), Oxygen (Z = 8), Silicon (Z = 14) and Phosphorous (Z = 15), this scattering is likely to occur.

The X-ray absorption edge of P-Kβ line is 2.140keV and the energy of Rh-Lα line from the X-ray tube (incident radiation) is 2.696keV. Considering that a fraction of the photons from the incident radiation undergoes inelastic scattering, they lose energy being capable to reach values suffice close than the absorption edges corresponding to the Phosphorous.

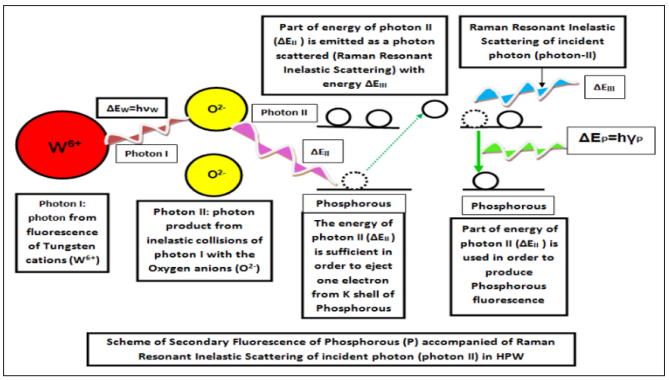


**Figure 32:** Proposed scheme of the Secondary Fluorescence of Phosphorous and X-ray Raman Resonant Scattering in $H_3PW_{12}O_{40}$

Another process that could be considered is the Auger radiative effect, which according to the reported by Van Espen et al (1979) could be of importance for the application of analytical methods based on energy dispersive like EDXRF and PIXE. Maeda and Kawai reported the interference of the Auger radiative satellites lines on XRF traces analysis for elements with lower atomic numbers [20]. These authors showed that the satellite Auger line KLL reaches from 0.8 to 1.5% of the intensity of the Kα line, and the satellite line Auger KMM reaches from 5.0 to 10% of the intensity of the Kβ line [31]. These intensities ratios (Intensity of satellite Auger line / Intensity of XRF K-line) are important in order to perform quantitative analysis, when the concentration of the element analyzed (Phosphorous in our case) is present in trace level (<1% m/m). In our study, the nominal concentration of Phosphorous is 0.5%, so the influence of the Auger effect is to be take in consideration.

In the Table 8 are presented the XRF lines in the energy range from 2.0 to 2.4 keV, corresponding to the elements Phosphorous (P), Tungsten (W) and Rhodium (Rh), being this latter element the material of the X-ray tube at the EDXRF spectrometer. Analogously, in the Table 9 are presented the XRF lines in the energy range from 2.0 to 2.9 keV, corresponding to the elements Phosphorous (P), Molybdenum (Mo) and Rhodium (Rh).

**Table 8: XRF lines for W, P and Rh in the energy range 2.0-2.4 keV**

| Element | XRF Line | Energy(keV) |
|---|---|---|
| Tungsten | $WM_2N_4$ | 2.312 |
| Tungsten | $WM_1N_3$ | 2.388 |
| Rhodium | $RhL\alpha_1$ | 2.368 |
| Tungsten | $WM_3O_5$ | 2.286 |
| Tungsten | $WM_\gamma$ | 2.060 |
| Tungsten | $WM_3N_4$ | 2.034 |
| Phosphorous | $PK\alpha_1$ | 2.013 |
| Phosphorous | $PK\beta_1$ | 2.139 |

| Element | XRF Line | Energy(keV) |
|---|---|---|
| Molybdenum | $MoL\gamma_3$ | 2.825 |
| Molybdenum | $MoL\beta_3$ | 2.473 |
| Molybdenum | $MoL\beta_4$ | 2.455 |
| Molybdenum | $MoL\gamma_1$ | 2.611 |
| Molybdenum | $MoL\beta_1$ | 2.396 |
| Molybdenum | $MoL\beta_2$ | 2.508 |
| Molybdenum | $MoL\alpha_1$ | 2.295 |
| Molybdenum | $MoL\alpha_2$ | 2.291 |
| Molybdenum | $MoL_l$ | 2.016 |
| Rhodium | $RhL_1$ | 2.368 |
| Rhodium | $RhL\alpha_1$ | 2.698 |
| Rhodium | $RhL\alpha_2$ | 2.692 |
| Phosphorous | $PK\alpha_1$ | 2.013 |
| Phosphorous | $PK\beta_1$ | 2.139 |

**Table 9:** XRF lines for Mo, P and Rh in the energy range 2.0-2.9 keV

Considering the energy resolution of the spectrometer EDXRF (0.2 keV), there might be overlapping between the XRF lines of Phosphorous, Tungsten, and Rhodium, as was shown in Table 8. Thus, it would be fulfilling one of the requirements for the existence of X-Ray Resonant Raman Scattering: the energy value of the incident radiation (XRF line of Rhodium) is closer to the correspondent value of the absorption edge of the irradiated elements (Phosphorous and Tungsten). The energies of X-ray absorption edges for the Phosphorous XRF lines P-Kα and P-Kβ are 2.010keV and 2.140keV respectively; for the Tungsten XRF line W-Mα is 2.273 keV; and the energy of the incident radiation (from the Rhodium X-ray tube), correspondent to the XRF line Rh-$L_I$ is 2.368keV [21].

From Table 9, it is observed that there is more closeness of Molybdenum XRF lines than the Tungsten ones with the Rhodium lines. The energies correspondent to the X-ray absorption edges for the Molybdenum lines $MoL_{II}$ and $MoL_{III}$ are 2.628 and 2.523keV respectively, whereas the energy of the most intense Rhodium L line (RhLα1) is 2.698keV. Thus, the probability of X-ray Resonant Raman Scattering will be higher for Molybdenum than for Tungsten, because are involved the Molybdenum XRF L lines, which have higher fluorescence yields than the Tungsten M lines.

In order to argue this hypothesis, they are presented the Compton scattering peaks for Rhodium (Rh), obtained in the measurements of the ormosil films by WDXRF spectrometer RIX-3000 Rigaku:

| Element | Compton Line | Energy (keV) |
|---|---|---|
| Rhodium | $RhK\alpha_1$ | 7.858 |
| Rhodium | $RhK\beta_1$ | 2.063 |

**Table 10:** Rhodium Scattering Compton lines

**Discussion**

The results of experiments D and E (Figures 9 and 10 respectively) constitute evidence of self-absorption of the Tungsten fluorescence by Phosphorous in phosphotungstates ($[PW_{12}O_{40}]^{-3}$). This because the Tungsten intensity from ammonium paratungstate, which is not interfered by Phosphorous, is greater than the intensity from phosphotungstates (higher than approximately 100% in experiment D and 25% in the experiment E). The difference between the Tungsten mass percentages in phosphotungstates and paratungstates does not justify the different counting rates observed. It seems, therefore, that the chemical environment of the polyanion phosphotungstate is essential in order to understand this interference effect. In the Keggin structure of phosphotungstates, six Oxygen anions ($O^{2-}$) surround each Tungsten cation ($W^{6+}$) in a distorted octahedral arrangement. In total, this structure has 12 octahedra linked by $O^{2-}$. In the center of this structure four Oxygen anions ($O^{2-}$) surround the Phosphorous cation ($P^{5+}$), forming a Td symmetry. This cage structure of these polyanions favors the inelastic scattering of photons emitted from the $W^{6+}$ cations by the $O^{2-}$ anions neighbors. The central position of Phosphorous in the Keggin unit could benefit itself from the proximity to the $O^{2-}$ neighbors, and of its symmetry, absorbing the photons that experienced inelastic scattering, thus, producing the secondary fluorescence of Phosphorous.

The interference of Phosphorous in the X-Ray Fluorescence of Tungsten is probably due to self-absorption phenomenon according to the model illustrated in Figure 30. In this interference model for self-absorption, a portion of the photons emitted by the $W^{6+}$ cations undergoes inelastic collisions with the $O^{2-}$ anions, at the first coordination sphere of Tungsten in the phosphotungstates, and after these photons are absorbed by the P5+ cations, which in turn, emits characteristic X-ray photons. Therefore, there is a decrement in Tungsten intensity and in turn an enhancement in the Phosphorous intensity. **In order to do an** estimation of this effect, it is shown a procedure of calculation of the self-absorption of the main Tungsten XRF line (W-Lα) by the constituent elements of ormosil matrix (C, H, N, O, Si, P). The procedure consists of the following steps: a) Find an XRF line of the element of interest in wavelength units, (b) With this wavelength by values from tables or interpolation find the X-ray absorption coefficient for the elements in the matrix [22].

| Element | Mass fraction | Mass absorption coefficient μ[λ(W)] for λ(W)=1.4763Å | Mass absorption coefficient weighted μ[λ(W)] for λ(W)=1.4763Å |
|---|---|---|---|
| Si | 0.10 | 57.00 | 5.70 |
| O | 0.39 | 10.50 | 4.10 |
| C | 0.12 | 4.25 | 0.51 |
| N | 0.01 | 6.95 | 0.07 |
| H | 0.05 | 0.43 | 0.02 |
| P | 0.01 | 68.00 | 0.68 |

**Table 11:** Mass absorption coefficients for **the main XRF Tungsten line (W**-Lα, λ=1.47634Å)

From the Table 11, it can be seen that theoretically the Oxygen (O) and Silicon (Si) have a relevant participation (greater weighted absorption coefficient) in the absorption of Tungsten fluorescence line, in ormosil films containing phosphotungstates. Nevertheless, from our experimental results, the focus of self-absorption effect studied occurs mainly in the phosphotungstate structure. And since this structure does not experience drastic changes after the sol-gel process; it will be critical, in order to understand this effect, which element(s) is (are) closest to the Tungsten, because it (they) is (are) that (those) has (have) the greater probability of self-absorption of Tungsten fluorescence [1,2].

The amount of $O^{2-}$ ions in the structure of phosphotungstates ($[PW_{12}O_{40}]^{-3}$), and its proximity to the silicates network (constituted

by siloxanes and silanol) in ormosil is a key factor in order to explain this effect. According to it was reported by Elguera Ysnaga, the atoms that are more likely to absorb photons emitted by W6+ cations are the $O^{2-}$ anions present in the structure of phosphotungstates, after the $O^{2-}$ anions present in the siloxanes (-Si-O-Si-) and silanol (-Si-OH) network, and the Oxygen present in the organic groups constituting these materials.

The self-absorption of Tungsten and Molybdenum fluorescence by Phosphorous in mixed solutions of tungstates, molybdates and phosphates in the Experiments B and C is not of the same magnitude than the observed in ormosil films containing phosphotungstates, as was reported by Elguera Ysnaga. For instance, without these elements are not been sharing the same molecular structure and therefore, remain at very close distances, the self-absorption effect is minimal in the equivalent concentration ranges, of Phosphorous and Tungsten, existent in ormosil films. This dependence of the interference effect with the distance between $P^{5+}$ and $W^{6+}$ ions become even more evident when we look at Figures 5 and 7, when the concentration of Phosphorous or the moles ratio (P/W) and (P/Mo) are increased respectively. In fact, when one increases the concentration of Phosphorous, decreases the average distance between the $W^{6+}$, $Mo^{6+}$ and $P^{5+}$ ions, thereby increasing the likelihood of interaction between these species and, therefore, the self-absorption of Tungsten and Molybdenum fluorescence.

From the Figure 11, it can be observed the interference between the Tungsten W-LG4 line (LG line of the fourth order reflection, which possess 0.1% of the intensity of the main line W-Lα) and the Phosphorous P-Kα line. In our samples, the Phosphorous is a minority element (nominal concentration <1% m/m), and the Tungsten is a major element (nominal concentration > 40% m/m). Considering that, the fluorescence yield of Tungsten L lines is higher than the yield of the Phosphorous K lines, argues that this interference between P-Kα and W-LG4 lines has influence in the calculation of Phosphorous concentration. This superposition of lines cannot be observed in EDXRF measurements because their energy resolution is approximately 0.2keV. However, this interference is not of the same origin and magnitude that observed in EDXRF measurements.

From the XRF analyses of Phosphorous (K lines), Tungsten (M lines), and Molybdenum (L lines), as were shown in Tables 8 and 9; and also from the Compton scattering lines of Rhodium, in the energy range between 2.0-2.9keV, (see Table 10); we could infer the complexity of self-absorption of the Tungsten and Molybdenum fluorescence, in phosphotungstates ($[PW_{12}O_{40}]^{3-}$) and phosphomolybdates ($[PMo_{12}O_{40}]^{3-}$) respectively, by Phosphorous. For Molybdenum, the interference of Phosphorous is more pronounced than for Tungsten, because are involved the Mo-L lines, which have a greater fluorescence yield than the W-M lines. For phosphotungstates and phosphomolybdates is also probable the presence of the X-Ray Resonant Raman Scattering (XRRS), due to the proximity in energy of the Rhodium L lines (incident radiation) and the Phosphorous absorption edges (P-Kα and P-Kβ). As the nominal concentration of Phosphorous (P) in the ormosil films is less than 1% m/m, it can also be considered the interference of the satellites Auger lines, which could contribute in the increase in the intensity of this element.

From the Tables 6 and 7, we correlated in the region of 1.0-1.2Å, for ormosil samples, the distances correspondent to Zinc and Tungsten elemental (obtained by DRX). For this reason, it is possible that these species are present in the samples, even in a minor proportion. Taking in consideration that the elemental radius of Zinc and Tungsten are 1.39Å and 1.40Å respectively, both of these elements would be present in the samples [17]. For the existence of Tungsten elemental, the condition is the presence of lacunar structures of phosphotungstates, but these cannot be determined in ormosil [20]. Another possibility is the presence of Zn, which could be formed from the reduction of some $Zn^{2+}$ ions, able to be localized within the phosphotungstates structure.

From the Figure 21, it can be seen that in the range for R< 1.0 Å, the samples doped with $Ca^{2+}$ ions exhibit less oscillations, and resemble more to the PWA than the samples doped with $Zn^{2+}$ ions. Considering that the elemental radius of Calcium (1.97Å) is very different from the radius of Tungsten (1.40Å), one can deduce that is minimum the possibility of the presence of Ca within the phosphotungstates structure. Thus, the absence of Ca within this structure would justify the less oscillations than the ormosil doped with $Zn^{2+}$ ions.

The Fourier transform of the W-LIII-edge for ormosil samples doped with $Zn^{2+}$ and $Ca^{2+}$ cations (from 0.0Å to 5.0Å) show a greater number of oscillations than $H_3PW_{12}O_{40}$ (PWA). According to the literature, for Tungsten glasses the peaks at region between 2.0-4.0Å are attributed to the multiple-scattering effects (mainly) and to the single-scattering signals from Phosphorous and Tungsten atoms located in the second coordination shell [17]. From these observations, we could infer that for Tungsten the coordination number (chemical environment) for the first and second shell in the samples is greater than PWA, possibly by the presence of Zinc species. This later observation is based on from the similarity of the samples doped with $Zn^{2+}$ cations and $ZnWO_4$, in the distances range between 1.0-5.0Å, as was illustrated in the Figure 29.

## Conclusions

EDXRF measurements of ormosil films containing phosphotungstates ($[PW_{12}O_{40}]^{-3}$) showed that there is an inverse correlation between the concentrations of Phosphorous and Tungsten, or that the concentration of Phosphorous was overestimated and the concentration of Tungsten has been underestimated. In order to explain this phenomenon, they were performed studies of mixed solutions of phosphates and tungstates, which showed that this interference effect, at the concentration range existent in ormosil, is dependent on the molecular structure of the polyoxoanion. This dependence was confirmed by the XRF analysis of Ammonium paratungstate.

XRF measurements in ormosil, performed at laboratory equipment, showed us the self-absorption effect of the Tungsten fluorescence by Phosphorous in the phosphotungstates. However, in the extent that increase the Zn concentration in ormosil, the Phosphorous absorption effect decreases gradually.

Self-absorption/interference studies of Tungsten X-Ray fluorescence by the others constituents in the ormosil films led us to approach the XRF quantification not only from the atomic perspective, but also to supplement with the molecular approach. Studies done with molybdates solutions showed the same trend than tungstates ones, analogously, the Molybdenum intensities from phosphomolybdates solutions showed the same behavior as the Tungsten intensities from phosphotungstates solutions. From these results, we concluded that the structure of polyoxometalates (phosphotungstates and phosphomolybdates), containing Phosphorous as central atom, has influence on XRF analysis because the results obtained in tungstates and molybdates solutions, in the equivalent concentration range of Phosphorous and Tungsten in ormosil films do not simulate completely that was

observed in phosphotungstates. Only for concentrations around of 400 mol. $L^{-1}$ or higher, the tungstates and molybdates solutions start to resemble the phenomenon observed for phosphotungstates. This effect is justified because in the extent that the Phosphorous atoms are closer to Tungsten and/or Molybdenum ones, the probability of interaction between them will enhance. Thus, the interference of Phosphorous in X-ray Fluorescence of Tungsten and/or Molybdenum will be increase, thereby simulating the existing proximity of these elements in the molecules of the phosphotungstates and phosphomolybdates [23-33].

We proposed an interference model that takes into account the self-absorption of the Tungsten fluorescence by Phosphorous, the cage-shaped molecular structure (Keggin) of the polyanions and their distribution in the structure of ormosil. Considering that the Tungsten and Phosphorous main emission lines do not overlapping by EDXRF, were performed measures by WDXRF finding the superposition of Tungsten W-$L_{G4}$ and Phosphorous P-Kα lines, but that is not enough to justify our experimental observations. Therefore, we regarded an additional explanation, the X-Ray Resonant Raman Scattering produced by the $O^{2-}$ anions network in phosphotungstates, followed of the Phosphorous absorption of the inelastic scattered photons for the $O^{2-}$ anions. Thus, the interference does not occur primarily by direct self-absorption, but by a combination of inelastic scattering process followed by absorption.

Our results and estimates show that the X-ray Resonant Raman Scattering can occur in the XRF analysis of phosphotungstates and phosphomolybdates performed in spectrometers with Rhodium X-ray tube. This inelastic scattering would base on the contribution of the $O^{2-}$ anions network, generating the proximity in energy between the Rhodium L lines (incident radiation) with the absorption edge of Phosphorus, which is the principal condition for the existence of this scattering.

The increase in X-ray fluorescence of Phosphorous in phosphotungstates could be due to various phenomenon such as Secondary Fluorescence, X-ray Resonant Raman Scattering and by the contribution of radiative satellites Auger lines.

XANES and EXAFS measurements given evidence of intermolecular and intramolecular interaction between Zinc and Tungsten species.

From this table, it can be seen that the value of the Compton scattering line RhKβ1 (2.063KeV) is close to the Phosphorous XRF K lines, the Tungsten M lines and the Molybdenum L lines, which were shown in the Tables 8 and 9. This scattering line is almost coincident in energy with the WMγ line (2.060KeV) and MoLI line (2.016KeV). From these results, one can infer that the interference of the Phosphorous in the phosphotungstates ($[PW_{12}O_{40}]^{3-}$) and phosphomolybdates ($[PMo_{12}O_{40}]^{3-}$) is a complex phenomenon. This phenomenon involves the overlapping of XRF lines of Phosphorous, Tungsten, Molybdenum, and Rhodium. The XRF Rhodium lines are closer in energy with the X-ray absorption edges of Tungsten (M lines) and Molybdenum (L lines), arguing the possibility of the X-Ray Resonant Raman Scattering and also the overlapping of the lines and absorption edges already mentioned with the inelastic scattering (Compton) line of Rhodium.

**Acknowledgments**

The authors thank to the São Paulo Research Foundation, FAPESP (research grant 2011/08120-0). Orlando Elguera Ysnaga thanks to CNPq Brazilian agency by the financial support (research grants 141880/2011-2 and 160515/2011-4); to Dr. Vera Luzia Salvador, Dr. Ivone Sato and Dr. Marcos Scapin for the WDXRF measurements with the Rigaku RIX3000 spectrometer at Laboratory of X-ray Fluorescence (XRF) of the Centro de Química e Meio Ambiente (CQMA) from (IPEN/CNEN-SP); to Dr. Anna Paula S. Sotero Levinsky for her assistant in the XANES/EXAFS measurements done at LNLS; to the CNPEM-LNLS, Campinas-Brazil for the realization of XAFS experiments, proposals number: XAFS1 15185; to Prof. Dr. Valmor Mastelaro of the Instituto de Física de São Carlos from the Universidade de São Paulo (IFSC-USP) for his help in the EXAFS fitting (Figure s), to the Dr. Akihito Iwata and to Mr. Ricardo Peixoto for his collaboration in the EDXRF/ WDXRF measurements done at Laboratory of X-ray Diffraction and X-ray Fluorescence of the Rigaku-São Paulo-Brazil, to Prof. Dr. Jun Kawai of Kyoto University-Japan.

**References**

1. Gonçalves LP (2011) Titanium nanoparticles as additives in photochromic inorganic hybrid materials based on phosphotungstates. São Carlos, São Paulo-Brazil: São Carlos Institute of Chemistry/ São Carlos School of Engineering, University of São Paulo (EESC-USP/ IQSC-USP) https://oasisbr.ibict.br/vufind/Record/USP_b1852d308b0f838f38172b28a7a6e781.
2. Paiva Ferreira Neto E (2011) Preparation, Characterization and Photochromic Behavior of Ormosyl-Phosphotungstate Hybrid Films doped with ZnO Nanoparticles. São Carlos, São Paulo-Brazil: Institute of Chemistry of São Carlos, University of São Paulo (IQSC-USP).
3. Elguera Ysnaga OA (2015) Methods of Analysis of Hybrid Materials: A comparative study between X-ray Fluorescence with Energy Dispersive Detection using Traditional Source and Synchrotron Light. São Carlos, São Paulo-Brazil: Institute of Chemistry of São Carlos, University of São Paulo (IQSC-USP) 249-301.
4. Meisel A, Leonhardt G, Szargan R (1989) X-ray Spectra and Chemical Binding. Berlin: Springer-Verlag 37.
5. Liebhafsky H, Pfeiffer H, Winslow E, Zemany P (1960) X-ray Absorption and Emission in Analytical Chemistry. New York: Editorial John Wiley 357.
6. Hoffmann R (1989) Solids and Surfaces: A Chemist's View of Bonding in Extended Structures. Wiley 1-160.
7. Compton A, Allison S (1967) X-rays in Theory and Experiment. Chicago: D.Van Nostrand Company Inc 828.
8. BLocH F (1935), Double Electron Transitions in X-ray Spectra. Physical Review 48.
9. Sparks C (1974) Inelastic Resonance Emission of X-rays: Anomalous Scattering Associated with Anomalous Dispersion. Physical Review Letters 33: 262-265.
10. Åberg T, Utriainen J (1969) Evidence for a "Radiative Auger Effect" in X-ray Photon Emission. Physical Review Letters 22: 1346-1348.
11. Åberg T (1971) Theory of the Radiative Auger Effect. Physical Review Letters 4: 1735-1740.
12. Szlachetko J (2007) X–ray Resonant Raman scattering in light elements and Relative detection efficiency of Charge Coupled Devices. Département de Physique-Université de Fribourg, Suisse https://folia.unifr.ch/unifr/documents/303143.
13. Yigal B, Freund I (1975) Resonant X-ray Raman Scattering. Physical Review Letters 34: 372-376.

14. Schülke W (2007) Electron Dynamics Studied by Inelastic X-ray Scattering. Oxford University Press 606.
15. Bergmann U, Glatzel P, Cramer S (2002) Bulk-sensitive XAS Characterization of Light Elements: from X-ray Raman Scattering to X-ray Raman spectroscopy. Microchemical Journal 71: 221-230.
16. Sánchez H, Valentinuzzi M, Leani J (2012) Theoretical Calculations of the Influence of Resonant Raman Scattering on the Quantification of XRF Spectrochemical Analysis. Journal of Analytic Atomic Spectrometry 27: 232-238.
17. Kawai J, Ohta M, Konishi T (2010) Chemical Effects in High Resolution Nickel Kα X-ray Fluorescence Spectra. Analytical Sciences - The Japan Society for Analytical Chemistry 21: 865-868.
18. Souza ALD, Carvalho FLSD, Schneider JF, Pereira RU (2010) Photochromic formulation, photochromic optical elements and their preparation process and use of the photochromic optical element https://repositorio.usp.br/single.php?_id=002246843&locale=pt_BR.
19. Ferreira-Neto EP, de Carvalho FLS, Ullah S, Zoldan VC, Pasa AA, et al. (2013) Surface structure and reactivity study of phosphotungstic acid-nitrogenated ormosils. J Sol-Gel Sci Technol 66: 363-371.
20. Maeda K, Kawai J (1993) Interfering Line in Trace Analysis by X -ray Spectrometry: Radiative Auger Satellites. Advances in X-ray Analysis Japan 25: 25-38.
21. National Physical Laboratory. Tables of Physical & Chemical Constants, Section 4: Absorption of Photons/X-Ray Absorption Edges, Characteristic X-Ray Lines and Fluorescence Yields http://www.kayelaby.npl.co.uk/atomic_and_nuclear_physics/4_2/4_2_1.html.
22. Jenkins R, De Vries B (1970) Worked Examples in X-ray Spectrometry. Philips Technical Library Netherlands 80-91.
23. Wright JD, Sommerdijk NAJM (2000) Sol-Gel Materials: Chemistry and Applications (1st ed.). Advanced Chemistry Texts (Inglés). CRC Press https://www.taylorfrancis.com/books/mono/10.1201/9781315273808/sol-gel-materials-nico-sommerdijk-david-phillips-stanley-roberts-paul-brien-john-wright.
24. de Oliveira M, Rodrigues-Filho UP, Schneider J (2011) Local Structure and Photochromic Response in Ormosils containing Dodecatungstophosphoric Acid. Chemistry of Materials 23: 953-963.
25. Silva De Carvalho F (2008) Effect of Matrix on the Photochromic Behavior of Phosphotungstate Ormosils. 2008.104f. Master's Dissertation - Institute of Chemistry of São Carlos, University of São Paulo, São Carlos.
26. Klockenkämper R (1997) Total Reflection X-ray Fluorescence Analysis and Related Methods. In: Chemical Analysis: A Series of Monographs on Analytical Chemistry and Its Applications. New York: John Wiley, 1st Edition 140.
27. Jenkins R (1999) X-ray Fluorescence Spectrometry. Chemical Analysis New York: John Wiley 152.
28. Dziunikowski B (1989) Energy Dispersive X-ray Fluorescence Analysis. Comprehensive Analytical Chemistry v. xxiv. Warszaw: Elsevier 431.
29. Buhrke V, Jenkins R, Smith D (1998) A Practical Guide for the Preparation of Specimens for X-ray Fluorescence and X-ray Diffraction Analysis. New York: John Wiley & Sons 334.
30. Conradson SD (2000) XAFS: A Technique o Probe Local Structure. Los Alamos Science 26: 422-435.
31. Aksenov VL, Ywkuznon A, Puranj J, Tyutyunnivov SI (2001) EXAFS Spectroscopy at Synchrotron-Radiation Beams. Kurchatov Institute of Atomic Energy Physics of Particles and Nucleus 32: 1.
32. Kuzmin A, Purans J (1997) X-ray Absorption Spectroscopy Study of the Local Environment around Tungsten and Molybdenum. Institute of Solid-State Physics, University of Latvia, Latvia. Proceedings of SPIE (Proc. SPIE) 180-185.
33. Karapetiants M, Drakin S (1974) Structure of substance. Mir Publishing House, Moscow 114.